https://doi.org/10.5194/egusphere-2025-3177
Preprint. Discussion started: 11 July 2025

Meteorological Drivers of the Low-Cloud Radiative Feedback Pattern Effect and its Uncertainty

Rachel Yuen Sum Tam[1], Timothy A. Myers[2,3], Mark D. Zelinka[4], Cristian Proistosescu[1,5], Yuan-Jen Lin[6,7], and Kate Marvel[7]

[1]Department of Atmospheric Science, University of Illinois at Urbana-Champaign, Urbana, IL, USA
[2]Cooperative Institute for Research in Environmental Sciences, University of Colorado, Boulder, CO, USA
[3]Physical Sciences Laboratory, National Oceanic and Atmospheric Administration, Boulder, CO, USA
[4]Lawrence Livermore National Laboratory, Livermore, CA, USA
[5]Department of Earth Sciences and Environmental Change, University of Illinois at Urbana-Champaign, Urbana, IL, USA
[6]Center for Climate Systems Research, Columbia University, New York, NY, USA
[7]NASA Goddard Institute for Space Studies, New York, NY, USA

Correspondence: Rachel Yuen Sum Tam (rytam2@illinois.edu)

Abstract. The radiative feedback pattern effect remains a large source of uncertainty for both projections of future trends and interpretations of past trends in global temperature. The pattern effect is defined as the difference in feedbacks between transient and long-term simulations, and past work shows that is primarily attributed to changes in the marine low-cloud radiative feedback. Here we use low cloud meteorological kernels to map out both the primary cloud controlling factors through which changing surface temperature patterns drive changes in low-cloud feedback, as well as the sources of model spread. We find that the pattern effect is almost entirely driven by changes in EIS in the Southern Hemisphere, particularly in the South East Pacific and Southern Ocean. In both past and future simulations, inter-model spread is primarily caused by model differences in the sensitivity of low clouds to the environmental conditions, rather than differences in the simulated evolution of environmental conditions.

1 Introduction

The pattern effect refers to how the net radiative feedback changes as the pattern of surface warming evolves. The time-evolution of the net radiative feedback was first identified within general circulation model (GCM) simulations, where the feedback becomes less negative over time, leading to an increase in climate sensitivity (e.g. Senior and Mitchell, 2000; Held et al., 2010; Andrews et al., 2012; Armour et al., 2013; Andrews and Ringer, 2014; Armour, 2017; Proistosescu and Huybers, 2017). This evolution of radiative feedback is termed the "pattern effect" as it is driven by changes in the spatial pattern of warming (Armour et al., 2013; Andrews et al., 2015; Zhou et al., 2016, 2017; Dong et al., 2019). The magnitude of the pattern effect remains a large source of uncertainty for both interpretations of past trends (Armour et al., 2024) and projections of future changes in global temperature (Sherwood et al., 2020).

The change in the net feedback is primarily caused by changes in the shortwave cloud radiative feedback associated with marine low clouds (Andrews et al., 2015; Zhou et al., 2016). GCM experiments forced by abruptly quadrupling CO_2 show

https://doi.org/10.5194/egusphere-2025-3177
Preprint. Discussion started: 11 July 2025

that warming is initially delayed in certain regions, most notably the eastern tropical Pacific and the Southern Ocean. On long time scales however, these regions exhibit amplified warming. As these regions eventually warm, they actuate more positive radiative feedbacks. The primary atmospheric mechanism posited is that surface warming in regions of deep convection like the Indo-Pacific Warm Pool warms the troposphere and thus increases outgoing radiation through both the lapse rate feedback, and through increases in low-cloud cover mediated by changes in tropospheric stability (Dong et al., 2019; Zhou et al., 2016, 2017). In contrast, warming in regions of descent, like the eastern tropical Pacific, and other locations like the Southern Ocean, generally have a more local effect on top-of-atmosphere (TOA) radiation, and contribute to a less-negative global feedback through both lapse rate and cloud feedbacks.

Here we map out the primary cloud controlling factors (CCFs) that drive low-cloud feedbacks under changing surface temperature patterns and evaluate the sources of model spread in low-cloud feedback estimates. Section 2 details the methodology, with subsections detailing the GCM simulations used, CCF framework and choice of CCFs, sensitivities of low-cloud radiative anomalies or radiative effects to local meteorology - known as *meteorological cloud radiative kernels*, and the inter-model variance analysis. Section 3 explains global feedback and the spatial pattern quantified by meteorological kernels and the CCFs. We summarize the results in Section 4.

2 Cloud Controlling Factors and the Meteorological Cloud Radiative Kernels Framework

2.1 GCM Simulations

We use global climate model simulations from the Coupled Model Intercomparison Project CMIP Phase 5 (Taylor et al., 2012) and 6 (Eyring et al., 2016), totaling to 16 GCMs (Table E1). We analyze atmosphere-only historical simulations (*AMIP*), coupled historical simulations (*historical*), and coupled simulations with abrupt-quadrupling of atmospheric CO_2 (*abrupt-4xCO2*).

The *AMIP* and *historical* experiments are both analyzed over the 1982-2008 interval. While they both have forcing constituents consistent with the historical record, they differ in their boundary conditions and active components: *AMIP* is an atmosphere-only simulation with prescribed sea surface temperature and sea ice concentration variations, and the *historical* experiment has both ocean and atmosphere components active. Since coupled models struggle to reproduce trends in historical SST patterns, (Dong et al., 2021; Wills et al., 2022), the comparison between *AMIP* and *historical* is necessary to assess how the pattern effect driven by observed SST is different from the one in coupled GCM simulations.

We also use the idealized *abrupt-4xCO2* experiment to evaluate how future feedbacks will evolve as warming patterns change over time. *Abrupt-4xCO2* is a coupled ocean-atmosphere simulation wherein atmospheric CO_2 concentration is abruptly quadrupled at the initiation of the run and then kept constant for the entire duration of the run, which is typically 150 years long. All other forcings are kept at pre-industrial levels. We separate the first 20 and latter 130 years as an analog to the fast and slow climate response as (following, e.g., Andrews et al., 2015; Dong et al., 2020), and refer these two intervals as *4xCO2-fast* and *4xCO2-slow*.

https://doi.org/10.5194/egusphere-2025-3177
Preprint. Discussion started: 11 July 2025

2.2 Cloud Controlling Factors

Marine low cloud feedbacks remain a significant challenge for climate models, and explain a majority of inter-model spread in the total feedback estimate (Bony and Dufresne, 2005; Zelinka et al., 2020). To understand the drivers of marine low cloud feedbacks and attendant sources of uncertainty, we use the *Cloud Controlling Factor* (CCF) framework (e.g. review by Klein et al., 2017). The CCF framework partitions the low-cloud feedback into the product of the sensitivities of low-cloud radiative fluxes to a number of local CCFs indicative of local meteorology, and the changes in these local CCFs with global temperature change. The marine low cloud feedback can thus be written as:

$$\lambda_{low} = \frac{dR_{low}}{dT_g} = \sum_i \frac{\partial R_{low}}{\partial CCF_i} \frac{dCCF_i}{dT_g}, \tag{1}$$

where R_{low} represents local anomalies in the low-cloud radiative effect as will be discussed below, T_g represents global-mean temperature, and thus dR/dT_g represents local low-cloud feedbacks. $\partial R/\partial CCF_i$ represent the radiative sensitivities of low-clouds to each CCF, i, and are known as the *meteorological cloud radiative kernels* (Scott et al., 2020; Myers et al., 2021). Finally, $dCCF_i/dT_g$ are the sensitivities of CCFs to global surface temperature change. All terms in equation 1 are a function of latitude and longitude, except T_g. The global-mean low-cloud feedback can be estimated by summing all local responses. Since the meteorological kernels are local, they are invariant to changes in the pattern of surface warming. The impact of warming patterns shows up in the sensitivity of local CCFs to global warming, with different warming patterns yielding different values for $dCCF_i/dT_g$.

Changes in CCFs with temperature, $dCCF/dT_g$, are calculated by computing a linear trend in the CCF and a linear trend in temperature, and then dividing the two. We choose this approach over the standard approach of regressing CCFs directly against temperature due to recent work showing that the standard approach strongly aliases natural variability into feedback estimates (Lin et al., 2025). While pattern effects associated with natural variability are interesting in their own right (Proistosescu et al., 2018), our focus here is on feedback differences between transient and long-term warming induced by external forcing.

The 6 CCFs chosen in this study follow Scott et al. (2020) and Myers et al. (2021, 2023) and include sea surface temperature (SST), estimated inversion strength (EIS) - a measure of lower tropospheric stability, horizontal surface temperature advection (T_{adv}), relative humidity at 700hPa (RH), vertical velocity at 700hPa (ω), and near-surface wind speed (WS). Prior observational, model, and theoretical studies have documented in depth how CCFs impact marine boundary layer cloudiness (Klein et al., 2017; Lilly, 1968; Bretherton, 2015; Cesana and Del Genio, 2021; Myers and Norris, 2015; Scott et al., 2020).

2.3 Meteorological Cloud Radiative Kernels

Low-cloud meteorological cloud radiative kernels are the sensitivities of low cloud radiative effects to perturbations in the local large-scale environment, and have been used to provide observationally constrained estimates of the net low-cloud feedback and of the low-cloud feedback pattern effect (Myers et al., 2023). Since marine boundary layer clouds respond to large-scale environmental changes on the timescale of days, there is sufficient data in the satellite record to observationally constrain these kernels (Lewis et al., 2023; Mauger and Norris, 2010; Pincus et al., 1997; Scott et al., 2020).

https://doi.org/10.5194/egusphere-2025-3177
Preprint. Discussion started: 11 July 2025

Low-cloud fraction perturbations from either observational product (Scott et al. (2020), hereafter S20) or climate models (Myers et al. (2021), hereafter M21) are first convolved with the atmospheric flux sensitivities to cloud fraction perturbations, known as *cloud radiative kernels* (derived in Zelinka et al. (2012), modified for observations in Zhou et al. (2013)), to obtain time series of monthly low-cloud radiative anomalies (R_{low}). Meteorological cloud radiative kernels, ($dR_{low}/dCCF_i$), are then calculating through multi-linear regression of the R_{low} anomalies onto the CCFs.

The GCM kernels used in this study are derived by M21 using the same 7 CMIP5 models and 9 CMIP6 models detailed in Table E1 in Appendix E, primarily determined by the availability of cloud fraction histograms produced by the International Satellite Cloud Climatology Project (ISCCP) simulator (Bodas-Salcedo et al., 2011). Observational kernels derived by S20 used cloud properties and radiation data from NASA Clouds and the Earth's Radiant Energy System Flux by Cloud Type dataset (CERES-FBCT) (Doelling, 2020), the Collection 6.1 of the MODIS cloud products (MODIS) (Platnick and Yang, 2015), International Satellite Cloud Climatology Project (ISCCP) (Rossow et al., 2017), and the Advanced Very High-Resolution Radiometer Pathfinder Atmospheres Extended (PATMOS-x) (Heidinger et al., 2014). Variations in meteorological fields are derived from the European Center for Medium-Range Weather Forecasts (ECMWF) Reanalysis v5 (ERA5) (Copernicus Climate Change Service, 2019a, b). The National Oceanic and Atmospheric Administration (NOAA) Optimum Interpolation (OI) product is used for the monthly SST fields (Huang et al., 2021). These radiative sensitivities to the large-scale environment cover the oceans over 60°N to 60°S at a 5°-by-5° scale. Further details of derivation and physical interpretation of these kernels are described in detail in S20 and M21 respectively.

2.4 Inter-model Variance Partition

To understand the sources of inter-model spread in the total low-cloud feedback we decompose equation (1) in terms of the model ensemble mean and deviations from the ensemble mean:

$$\frac{dR_{low}}{dT_g} = \sum_i \frac{\partial R_{low}}{\partial CCF_i}\frac{dCCF_i}{dT_g} = \sum_i \left(\overline{\frac{\partial R_{low}}{\partial CCF_i}} + \left(\frac{\partial R_{low}}{\partial CCF_i}\right)'\right)\left(\overline{\frac{dCCF_i}{dT_g}} + \left(\frac{dCCF_i}{dT_g}\right)'\right) \tag{2}$$

where the $\overline{x}$ notation represents the model ensemble mean, and the x' represents model-specific anomalies from the ensemble mean. We can estimate the low-cloud feedback dR_{low}/dT_g inter-model variance as below:

$$Var\left[\frac{dR_{low}}{dT_g}\right] = Var\left(\sum_i \left[\left(\frac{\partial R_{low}}{\partial CCF_i}\right)'\left(\overline{\frac{dCCF_i}{dT_g}}\right)\right]\right) + Var\left(\sum_i \left[\left(\overline{\frac{\partial R_{low}}{\partial CCF_i}}\right)\left(\frac{dCCF_i}{dT_g}\right)'\right]\right) + \epsilon. \tag{3}$$

Equation (3) quantifies how much of the total low-cloud feedback spread comes from, respectively, the model spread in the cloud radiative sensitivity to changes in CCFs, and the model spread in how GCMs simulate changes in CCFs in response to warming. ϵ is an error term due to potential covariance between the radiative flux sensitivity to meteorology and the meteorology, or between the sensitivities of different CCFs. An observationally-based set of meteorological kernels can also be used in place of the model ensemble mean kernels.

Using this framework, we build on the work of S20, M21 and Myers et al. (2023) to examine (1) the contributions of different CCFs to the cloud feedback pattern effect under various past and future climate change scenarios, (2) the major

https://doi.org/10.5194/egusphere-2025-3177
Preprint. Discussion started: 11 July 2025

sources of feedback uncertainty, and (3) how coupled model biases in the evolution of historical SSTs lead to biases in the feedbacks (Andrews et al., 2022).

3 Global and Regional Cloud Feedback Patterns

3.1 Global Feedback

Figure 1 presents the kernel estimate of the total marine low-cloud feedback and the sub-component contributions from each CCF. From the top to bottom, panels show the feedback calculated with a) both kernels ($\partial R_{low}/\partial CCF_i$) and changes in meteorologies ($dCCF_i/dT_g$) derived from models, showing the total model-spread in low-cloud feedbacks; b) observationally constrained kernels with model-specific changes in meteorology, showing the contribution to model spread from uncertainty in the meteorology and c) model-specific kernels and multi-model mean changes in meteorology, showing the contribution to model spread from uncertainty in kernels. A near-global marine low cloud feedback is computed using spatially-weighted averages of equation (1) across the oceans between 60°N-60°S, following S20 and M21. The color of the markers represents the different experiments, the red diamond indicates the multi-model mean, and the black line shows the ensemble standard deviation (1σ). The inter-experiment total low-cloud feedback mean values and standard deviation are included in Table F1 of Appendix F.

3.1.1 Ensemble Mean Results: Drivers of Low-cloud Feedback

Focusing on the ensemble mean (red markers in Figure 1a), we find that *AMIP* experiments have a negative (stabilizing) marine low-cloud feedback; *historical* have a near-zero feedback, *4xCO2-fast* have a weakly positive feedback, while *4xCO2-slow* have a slightly more positive feedback. These feedback estimates come with a large model spread that often crosses zero. However, individual models show similar differences between experiments as the ensemble mean, suggesting a consistent sign of the pattern effect across models.

Across the three experiments indicative of transient warming (*AMIP, historical, 4xCO2-fast*) the total marine low-cloud feedback is determined by a compensation between a negative contribution from EIS and positive contributions from SST and RH. On long time scales (*4xCO2-slow*) both the EIS and RH components are nearly zero, with the total feedback thus being determined almost entirely by the SST component. The other three CCFs, T_{adv}, ω, and WS have near zero contributions in the global-mean.

https://doi.org/10.5194/egusphere-2025-3177
Preprint. Discussion started: 11 July 2025

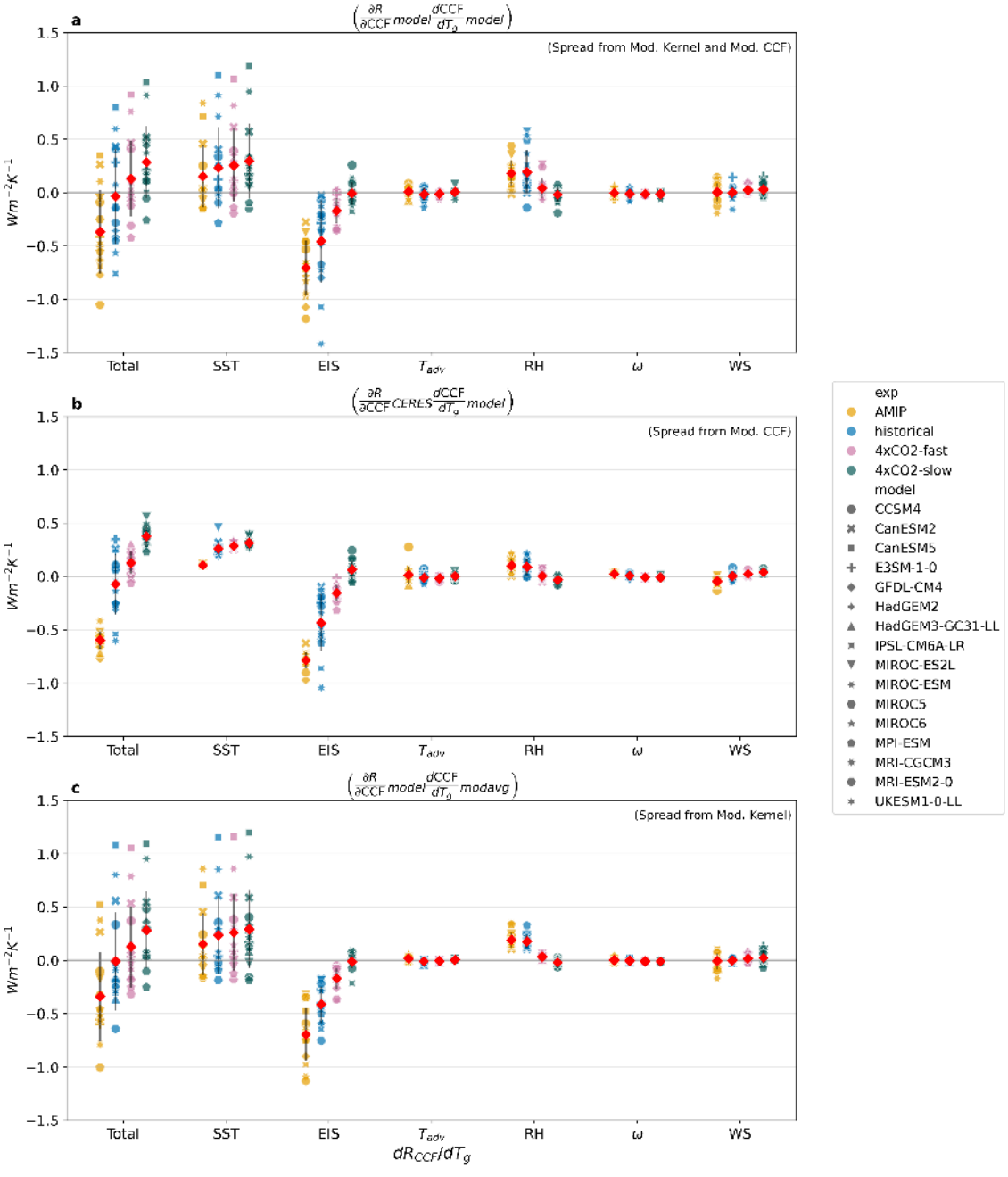

Figure 1. Marine-only, spatially-weighted averages of 60°N-60°S low-cloud feedback estimates and its sub-components using (a) **model-specific** radiative flux sensitivities to meteorological changes ($\partial R_{low}/\partial CCF$) and **model-specific** meteorological changes to warming ($dCCF/dT_g$), (b) radiative flux sensitivities to meteorology observationally constrained with the **CERES-FBCT product** and **model-specific** meteorological changes, and (c) **model-specific** radiative flux sensitivities to meteorology and **ensemble-averaged** meteorological changes.

https://doi.org/10.5194/egusphere-2025-3177
Preprint. Discussion started: 11 July 2025

Figure 1. (Cont.) Each marker represents one model estimate, where the model-ensemble average and ensemble standard deviation (1σ) are illustrated by the red diamond and the black line respectively.

The SST component is roughly constant across experiments. The EIS component is very strongly negative in *AMIP* simulations, with its value becoming progressively less negative across in the coupled *historical* and *4xCO2-fast* experiments. The contribution of RH is small but not insignificant in the *AMIP* and *historical* experiments and is nearly zero in both *4xCO2* experiments. The ensemble mean total low-cloud feedback is slightly negative in the *historical* experiment, but is slightly positive in the fast-response of the 4xCO2 experiment.

3.1.2 Ensemble Mean Results: The Pattern Effect

The marine low cloud contribution to the pattern effect can be computed as the difference in the feedback estimate between different experiments. All panels in Figure 1 show that the marine low-cloud feedback becomes less negative as we go from transient *AMIP*, *historical*, and *4xCO2-fast* simulations to the *4xCO2-slow* simulation representative of the long-term response. Our kernel-derived estimates are thus consistent with past literature on the pattern effect, suggesting the low-cloud feedback evolves to be less negative over time (Andrews et al., 2015, 2018, 2022; Myers et al., 2023).

The CCF decomposition shows that the pattern effect is driven almost entirely by changes in the EIS component feedback. Both ensemble means and most individual models agree that EIS components are strongly negative in *AMIP* and *historical* experiments, and weakly negative in *4xCO2-fast*, eventually becoming near zero on long time scales in *4xCO2-slow*. The SST-component is similar in magnitude across all experiments, which means it has a minimal contribution to the pattern effect. The RH-component becomes less positive in the *4xCO2-slow* compared to the transient simulations, leading to a small compensation of the much larger EIS-induced pattern effect.

It is worth noting the difference in feedbacks between *AMIP* and the coupled simulations. Observed transient SST patterns drive both a slightly less positive SST-induced feedback and a more negative EIS-induced feedback (*AMIP*, indicated by yellow markers) than their coupled-model counterparts (*historical* and *4xCO2-fast*, indicated by blue and magenta markers) in Figure 1. This is consistent with coupled models having large systematic biases in equatorial Pacific SST patterns, where they are unable to reproduce the strengthening of the equatorial Pacific SST gradient and Walker Circulation as in observations (Wills et al., 2022). The weaker SST gradient in coupled-models generates a much weaker EIS signal (Dong et al., 2019).

Feedback induced by other CCFs (T_{adv}, ω, WS) have much smaller magnitudes or are near zero across experiments, contributing very little to the total low-cloud feedback in each experiment and the pattern effect.

3.1.3 Ensemble Mean Results: Observationally Constrained Low-cloud Feedback Estimates

We also show estimates of observationally constrained marine-low cloud feedbacks using CERES-FBCT kernels in Figure 1b, and MODIS, ISCCP and PATMOS-X products (Figure A1). The overall pattern of the total feedback and its components using observational kernels is similar to that using model-specific kernels. All results using observationally-derived kernels

https://doi.org/10.5194/egusphere-2025-3177
Preprint. Discussion started: 11 July 2025

suggest a weak negative total low-cloud feedback in the *historical* experiment, except results calculated with the PATMOS-X kernels, suggesting a weak positive total low-cloud feedback driven by a stronger-than-model SST-induced feedback and a weaker-than-model EIS-induced feedback. *4xCO2-fast* and *4xCO2-slow* total-low cloud feedback estimates are consistent across kernel choices, are weakly positive and positive respectively. While the overall pattern stays the same, the magnitudes of observationally-constrained feedback are sensitive to the choice of kernels, particularly in the *AMIP* simulations. For example, the ensemble-mean transient total low-cloud feedback in *AMIP* ranges from $\sim -1 W m^{-2} K^{-1}$ using MODIS-kernels to $\sim -0.25 W m^{-2} K^{-1}$ using PATMOS-X kernels.

3.1.4 Inter-model Spread

Following equation 3, we can attribute the inter-model spread in the marine low-cloud feedback and its subcomponents to either the radiative flux sensitivities to meteorology (kernels) or the meteorological changes under warming. Figure 1b shows feedback estimates with model-specific changes in meteorology ($dCCF/dT_g$), but replacing model-specific kernels ($\partial R_{low}/\partial CCF$) with CERES-FBCT observational kernels. Figure 1c shows feedback estimates with model-specific kernels, but replacing model-specific changes in meteorology with the ensemble-mean. The spread of markers in the two calculations is therefore indicative of the inter-model spread in the environmental response per unit warming only (Fig. 1b), or the model spread in the sensitivities of low cloud radiative fluxes to their local environment (Fig. 1c).

Overall, models have less disagreement on CCF responses to warming than the radiative flux sensitivities to CCF changes. Thus, the CCF decomposition shows that the vast majority of the uncertainty in both the net marine low cloud feedback and the pattern effect comes from uncertainty in how marine low clouds respond to their local environment (i.e. model spread in kernels, Fig. 1c). By comparison, the model uncertainty in how meteorology changes with warming is much smaller (i.e model spread in CCF changes, Fig. 1b), with the notable exception of the *historical* experiment. These results hold if the CERES-FBCT observational kernels are replaced with either the ensemble mean kernels or other observational kernels (Fig. A1). In terms of specific CCFs, the largest sources of uncertainty are the sensitivities of clouds to SST and EIS, with smaller contributions from RH and WS, and negligible contributions from T_{adv} and ω.

The positive extremes (upper limit) of total low-cloud feedback estimates can be attributed to models having higher radiative flux sensitivities to SSTs, such as MIROC-ESM (CMIP5) and CanESM5 (CMIP6). This suggests that constraining the sensitivity of marine low-clouds to SSTs is key to estimating the upper limit of the total low-cloud feedback.

In contrast, the negative extremes (lower limit) of the transient total low-cloud feedback inter-model spread in Fig. 1a is attributable to EIS-induced feedback across all experiments representative of the rapid response (*AMIP*, *historical* and *4xCO2-fast*), portrayed by the yellow, blue and magenta markers in the EIS columns. Estimates of low-cloud feedback for *AMIP*, *historical* and *4xCO2-fast* in the EIS column are negative across choice of meteorological kernels and meteorology (Fig. 1 and Fig. A1), implying that all models agree EIS will induce a stabilizing transient feedback, but the magnitude range of the negative feedback, and thus of the pattern effect, remains large.

The only experiment where uncertainty in meteorology is comparable with uncertainty in radiative sensitivity is the coupled *historical* experiment. In particular, there is a large model spread in changes the $dEIS/dT_g$ term in *historical* experiments

https://doi.org/10.5194/egusphere-2025-3177
Preprint. Discussion started: 11 July 2025

(Fig. 1b, EIS column). The same spread is not observed in the historical *AMIP* experiments that are all run with the identical SST patterns. These results suggest differences in $dEIS/dT_g$ across the coupled experiments likely come from differences in how the different SST patterns drive different patterns of atmospheric circulation. It is worth noting that differences in SST patterns across coupled models to not drive big differences in the direct SST response (Fig. 1b, SST column).

Finally, we note that while inter-model variance becomes much smaller when using observational kernels, the estimate of the marine low-cloud feedback estimates is very sensitive to the choice of observational kernels (Fig. A1). It is also likely that the inter-model spread in CCF-response in coupled models may be higher in the entire CMIP5 and CMIP6 ensemble, compared to the subset of 16 models with ISCCP simulator output that were used here.

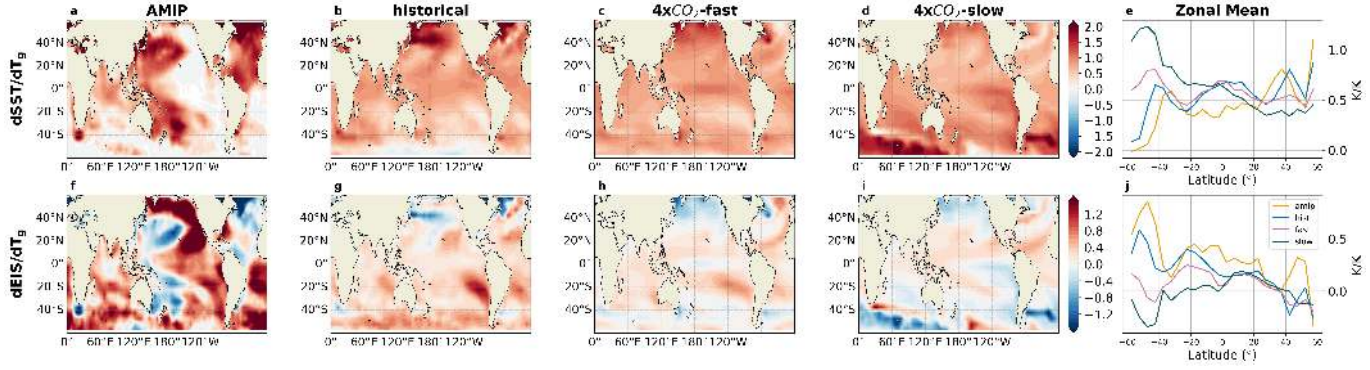

Figure 2. Spatial distribution and zonal averages of (a-e) SST and (f-j) EIS changes per degree warming in *AMIP*, *historical*, *abrupt-4xCO2-fast*, and *abrupt-4xCO2-slow* experiments. Yellow, blue, magenta and green lines in the zonal average plots represent *AMIP*, *historical*, *4xCO2-fast*, and *Slow* experiments. Units of colorbars are same as those in the zonal maps shown on the right. Maps of T_{adv}, RH, ω, and WS are shown in Supp. Fig. B1.

3.2 Regional Patterns

In this section, we analyze the spatial distribution of CCF-specific changes under warming and their induced low-cloud feedback. Figure 2 shows the ensemble mean changes of cloud-controlling factors per unit warming, $dCCF_i/dT_g$, and Figure 3, shows the low-cloud feedback induced by individual cloud-controlling factors, across experiments. We only show the feedback attributed to SST and EIS in the main figures for their larger role in driving the total low-cloud feedback and the low-cloud feedback pattern effect. The results for T_{adv}, RH, ω, and WS are shown in Fig. B1 and Fig. C1.

The three transient simulations show more warming in the West Pacific and either cooling (in *AMIP*) or less warming (in *historical* and *4xCO-fast*) in the Southeast Pacific and Southern Ocean, which eventually transitions to more warming in the East Pacific and Southern Ocean on long-time scales (*4xCO2-slow*). Despite these regional differences in SST, the direct contributions of SSTs to the low cloud feedback, dR_{SST}, are quite similar across experiments (Fig. 3). The AMIP simulation does show some significant regional differences for dR_{SST} especially in the North and Equatorial Pacific, but these cancel each other out when looking at zonal-mean (Fig. 3e) and global values (Fig. 1).

https://doi.org/10.5194/egusphere-2025-3177
Preprint. Discussion started: 11 July 2025

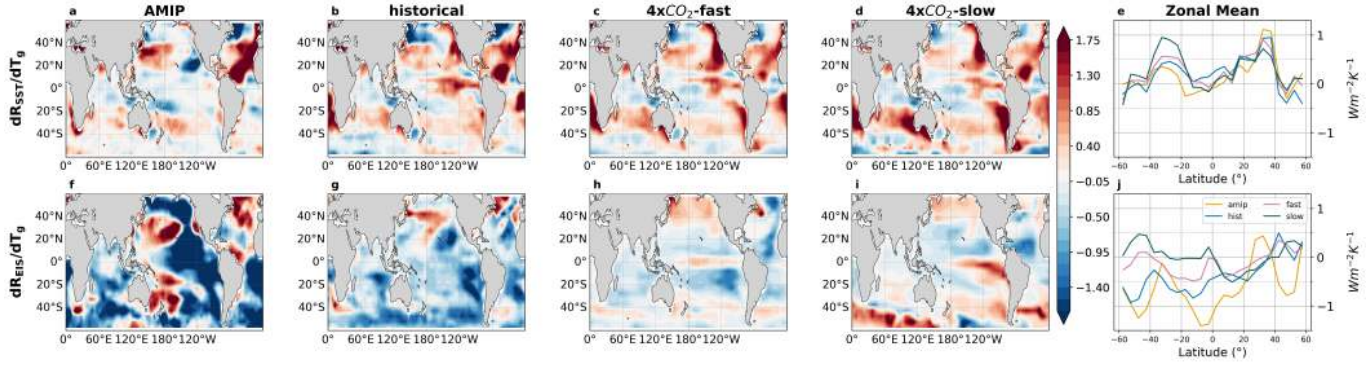

Figure 3. Spatial distribution and their zonal averages of ensemble mean (a-e) SST- and (f-j) EIS-induced feedback in AMIP, historical, abrupt-4xCO2-fast, and abrupt-4xCO2-slow experiments. Low-cloud feedback estimates are calculated using model-specific radiative flux sensitivities to CCFs and model-specific CCFs prior to taking multi-model mean. Yellow, blue, magenta and green lines in the zonal average plots represent *AMIP*, *historical*, *4xCO2-fast*, and *Slow* experiments. Units of colorbars are same as those in the zonal maps shown on the right. Maps of T_{adv}, RH, ω, and WS are shown in Supp. Fig. C1.

The different regional SST changes do, however, drive significant differences in marine low-cloud feedback through their impact on EIS patterns (Fig. 2f-j). EIS patterns go from exhibiting a strengthening of the inversion with global warming in the South East Pacific and the Southern Ocean in transient and historical simulations (*AMIP, historical, 4xCO2-fast*) to a weakening of the inversion with global warming in long term *4xCO2-slow*.

Overall, the changes in dR_{EIS} that dominate the pattern effect are primarily driven by the progressive weakening of the inversion in the low latitudes and in the South East Pacific between transient and long-term simulations (Fig. 3f-j). While the Northern Hemisphere exhibits strong regional changes in EIS and dR_{EIS}, these mostly cancel each other out in the zonal means (Fig. 3j).

Note that while the *AMIP* and coupled *historical* simulations share qualitative patterns of meteorology (e.g. Fig. 2a-b) and CRE changes (e.g. Fig. 3a-b), it is clear that coupled simulations struggle to replicate observed warming pattern and subsequent changes in meteorology and feedbacks. Large regional differences compensate each other in the SST component, such that zonal-mean and global-mean differences are negligible for dR_{SST}. However, these biases in SST patterns drive large biases in regional EIS, which in turn drive large biases in dR_{EIS}, that persist into the zonal- and global-means. The transient low-cloud feedback in *historical* is therefore biased-high and, holding the assumption that the *4xCO2-slow* response is representative of the future low-cloud response, the pattern effect is biased low.

Figure 4 maps inter-model spread in *regional* feedback estimates using equation (3). $Var(dR)$ maps the model spread of the total marine low-cloud feedback, $Var((\frac{\partial R}{\partial CCF})'\overline{dCCF})$ maps the spread of model kernels, and $Var(\overline{\frac{\partial R}{\partial CCF}}dCCF')$ maps the spread of meteorological condition changes, and the last column maps the residual term in the decomposition due to covariances between the first two terms.

https://doi.org/10.5194/egusphere-2025-3177
Preprint. Discussion started: 11 July 2025

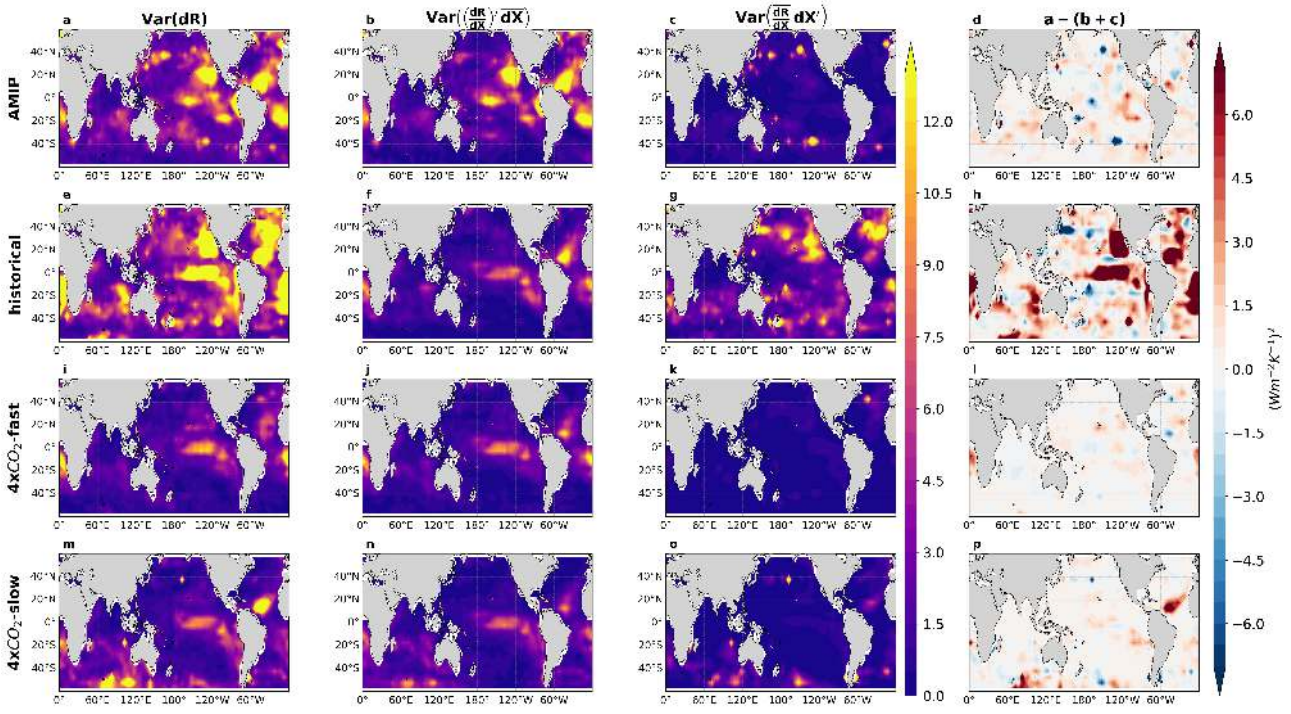

Figure 4. Spatial distribution (from left column to right) of the **total low-cloud feedback inter-model spread** and the breakdown of each term on the right-hand-side of Equation 3, including the variance determined by the **radiative flux sensitivities to CCF alone**, variance determined by **CCF changes from warming alone**, and the **covariance** between the *low-cloud meteorological kernels* and the meteorology for each experiment going from top to bottom row: (a-d) AMIP, (e-h) historical, (i-l) abrupt-4xCO2-fast and (m-p) abrupt-4xCO2-slow experiments. Spatial distribution for the inter-model spread for each CCF-induced feedback are shown in Supp. Fig. D1-D6.

As expected from the global analysis, there is high model agreement that most regional variance in the total feedbacks comes from the meteorological kernels (Fig. 4b, f, j, n), with the variance pattern in the model kernels largely mirroring the pattern in the total feedback variance (Fig. 4a, e, i, m). Results from *Historical* also have a high inter-model variance in the CCF changes per unit warming and covariance between the two terms, caused by the EIS-component as seen in Section 3.1 and Supp. Fig. D2. The regions with the largest spread in $Var(dR)$ are those with abundant marine low clouds. The central and eastern Pacific and tropical North Atlantic Ocean have low model agreement, with inter-model variance being dominated by the SST and EIS kernels (Fig. D1-6).

4 Summary and Conclusion

In this paper we identified changes in EIS (Fig. 1a) in the Southeast Pacific and Southern Ocean (Fig. 3j) as the largest contribution to the marine low-cloud pattern effect. The pattern effect is defined as the difference in feedback between transient and long-term warming, and results hold in an ensemble of 16 climate models, for three different estimates of transient warming:

https://doi.org/10.5194/egusphere-2025-3177
Preprint. Discussion started: 11 July 2025

atmosphere-only historical simulations (*AMIP*), coupled historical (*historical*) simulations, and the first 20 years of a coupled abrupt quadrupling simulation (*4xCO2-fast*).

Transient warming patterns are characterized by a strengthening of the inversion in the Southeast Pacific and Southern Ocean, which leads to a strong negative EIS-induced feedback. As the warming pattern evolves, EIS changes in these regions go from positive to negative, indicating an eventual weakening of the inversion, and a subsequent switch to a positive feedback in these regions.

Of the other CCFs, SST has a large contribution to the total marine low-cloud feedback, but that contribution is constant across experiments, leading to a negligible contribution to the pattern effect. RH changes between historical and long-term experiments suggest a small compensation of the EIS-induced pattern effect, while T_{adv}, ω, and WS have negligible contribution to both the net feedback and the pattern effect.

Additionally, we show that the majority of the uncertainty in the simulated low-cloud CRE lies in the model sensitivity of marine low clouds to environmental conditions, i.e. the meteorological kernels. However, a non-trivial amount of uncertainty does come from inter-model spread in how coupled models simulate historical changes in EIS. Since the spread in EIS is smaller for *AMIP* simulations with prescribed SSTs, the spread in EIS response in the coupled models must ultimately come from how coupled models simulate SST patterns, rather than the direct reponse of EIS to historical forcing. The impact of these differences in SST patterns on feedbacks is indirect, and shows up in the EIS-driven component, not in the SST-driven component. In addition to a large ensemble spread, coupled historical simulations also have a large bias relative to atmosphere-only historical simulations, due to their inability to capture observed SST patterns.

Our results help pinpoint the two main areas of future work needed to improve estimates of both the net marine low-cloud feedback and the pattern effect: a better constraint on the low-cloud response to inversion strength, and improved ability of coupled models to simulate historical SST patterns.

Code and data availability. The meteorological cloud radiative kernels are available at https://github.com/tamyers87/meteorological_cloud_radiative_kernels, with derivation method detailed in Scott et al. (2020) and Myers et al. (2021). All CMIP5 and CMIP6 model output are accessed from https://esgf-node.llnl.gov, with references of each dataset detailed and cited in Table E1. The code used to process and analyze the data is publicly available at https://github.com/rytam2/ccf_project.

https://doi.org/10.5194/egusphere-2025-3177
Preprint. Discussion started: 11 July 2025

Appendix A: Global feedback estimates calculated with meteorological kernels derived from other observations – MODIS, ISCCP, and PATMOS-X

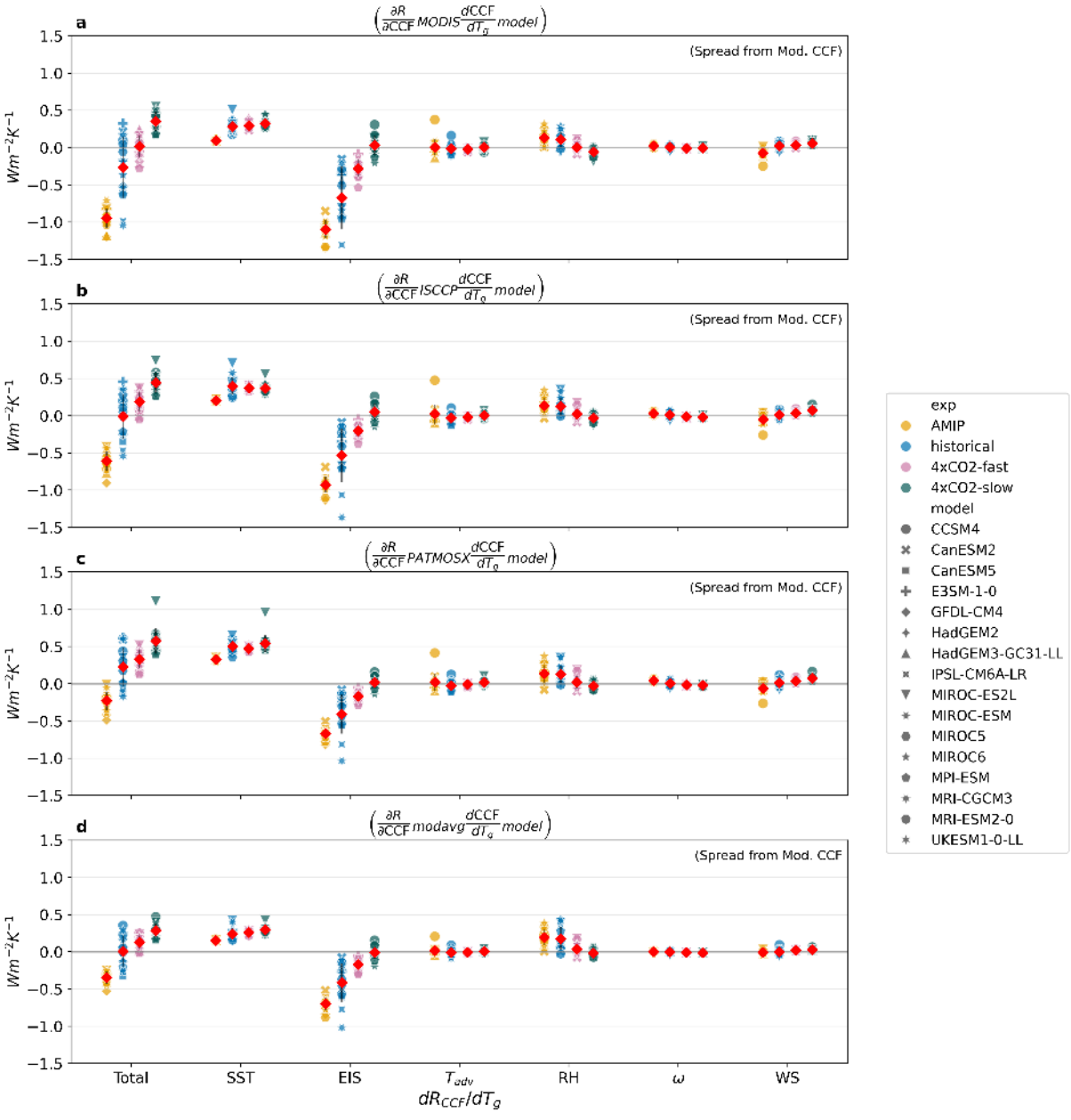

Figure A1. Marine-only, spatially-weighted averages of 60°N-60°S low-cloud feedback estimates and its sub-components calculated with radiative flux sensitivities to meteorology ($\partial R/\partial CCF$) derived from (a) **MODIS**, (b) **ISCCP**, (c) **PATMOS-x** products, and (d) **multi-model mean** and **model-specific** meteorological changes ($\partial CCF/\partial T_g$). Each model is represented by an individual marker.

https://doi.org/10.5194/egusphere-2025-3177
Preprint. Discussion started: 11 July 2025

Appendix B: Spatial maps of changes in subsidence (ω), and surface wind speed components (WS) for AMIP, historical, abrupt-fast and abrupt-slow experiments.

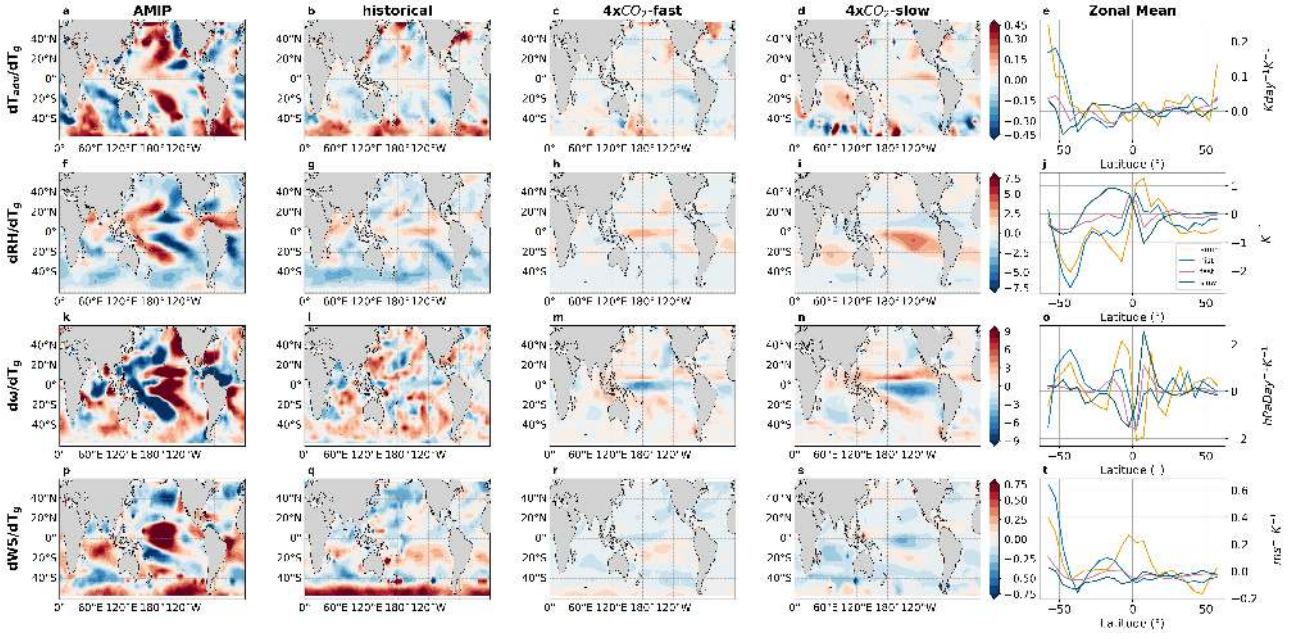

Figure B1. Spatial distribution and their zonal averages of (a-e) T_{adv}, (f-j) RH, (k-o) ω, and (p-t) WS changes per degree warming in *AMIP*, *historical*, *abrupt-4xCO2-fast*, and *abrupt-4xCO2-slow* experiments. Yellow, blue, magenta and green lines in the zonal average plots represent *AMIP*, *historical*, *4xCO2-fast*, and *4xCO2-slow* experiments.

https://doi.org/10.5194/egusphere-2025-3177
Preprint. Discussion started: 11 July 2025

Appendix C: Spatial maps of cloud feedback changes induced by changes in subsidence (ω), and surface wind speed components (WS) for AMIP, historical, abrupt-fast and abrupt-slow experiments.

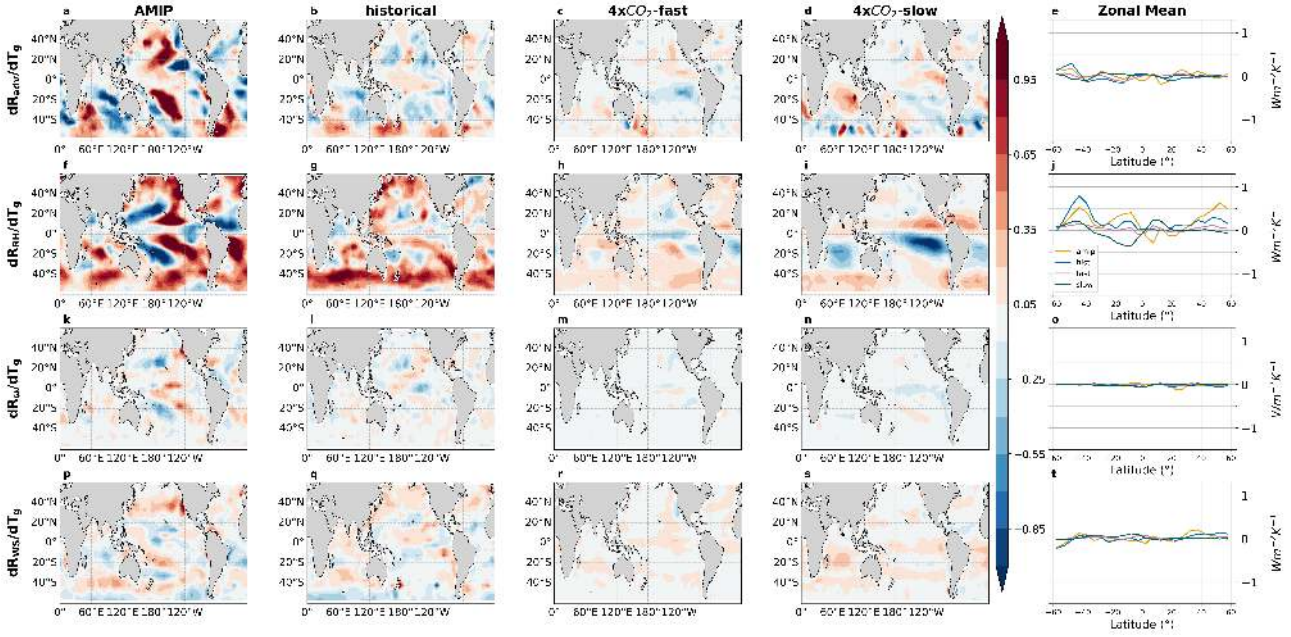

Figure C1. Spatial distribution and their zonal averages of (a-e) T_{adv}-, (f-j) RH-, (k-o) ω-, and (p-t) WS-induced feedback in *AMIP*, *historical*, *abrupt-4xCO2-fast*, and *abrupt-4xCO2-slow* experiments. Yellow, blue, magenta and green lines in the zonal average plots represent *AMIP*, *historical*, *4xCO2-fast*, and *Slow* experiments. Colorbar limits are tightened to better reflect the spatial pattern of the CCF-induced low-cloud feedback.

https://doi.org/10.5194/egusphere-2025-3177
Preprint. Discussion started: 11 July 2025

Appendix D: Variances from feedback induced by individual CCFs.

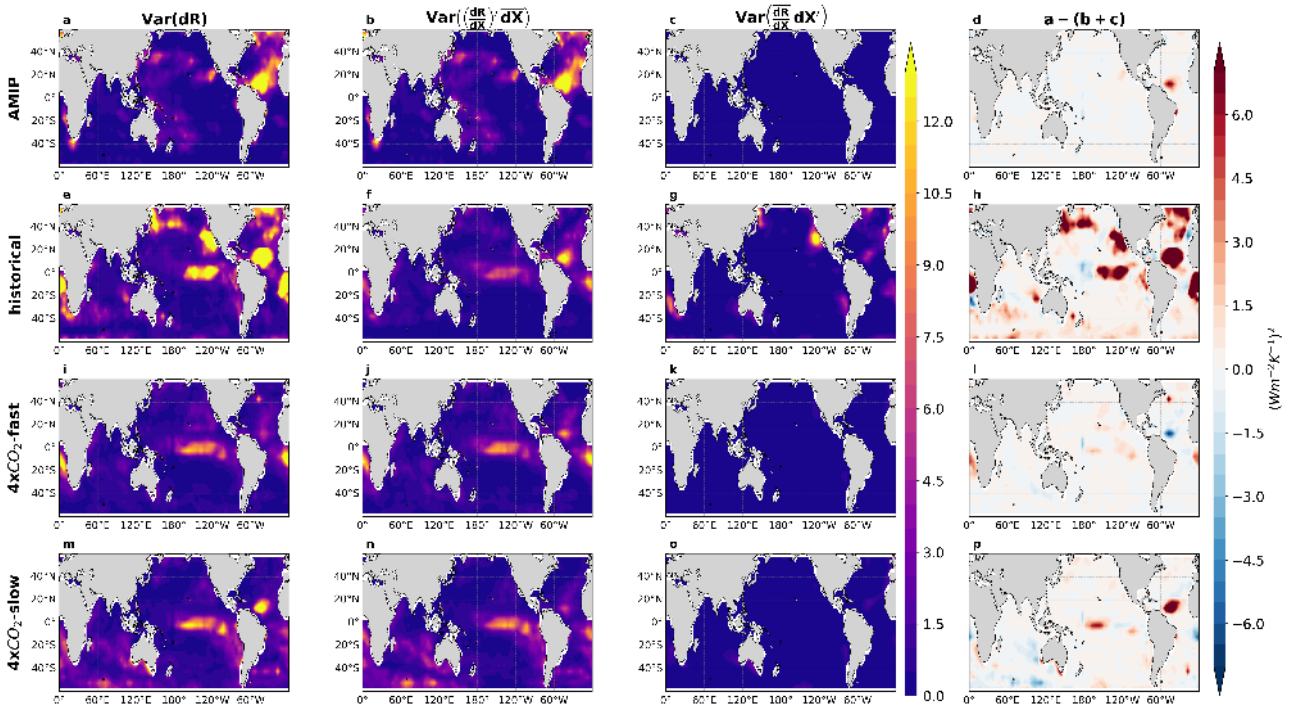

Figure D1. Same as Figure 4 on the spatial distribution of variance for each term in Equation 3 specific to SST-induced feedback.

https://doi.org/10.5194/egusphere-2025-3177
Preprint. Discussion started: 11 July 2025

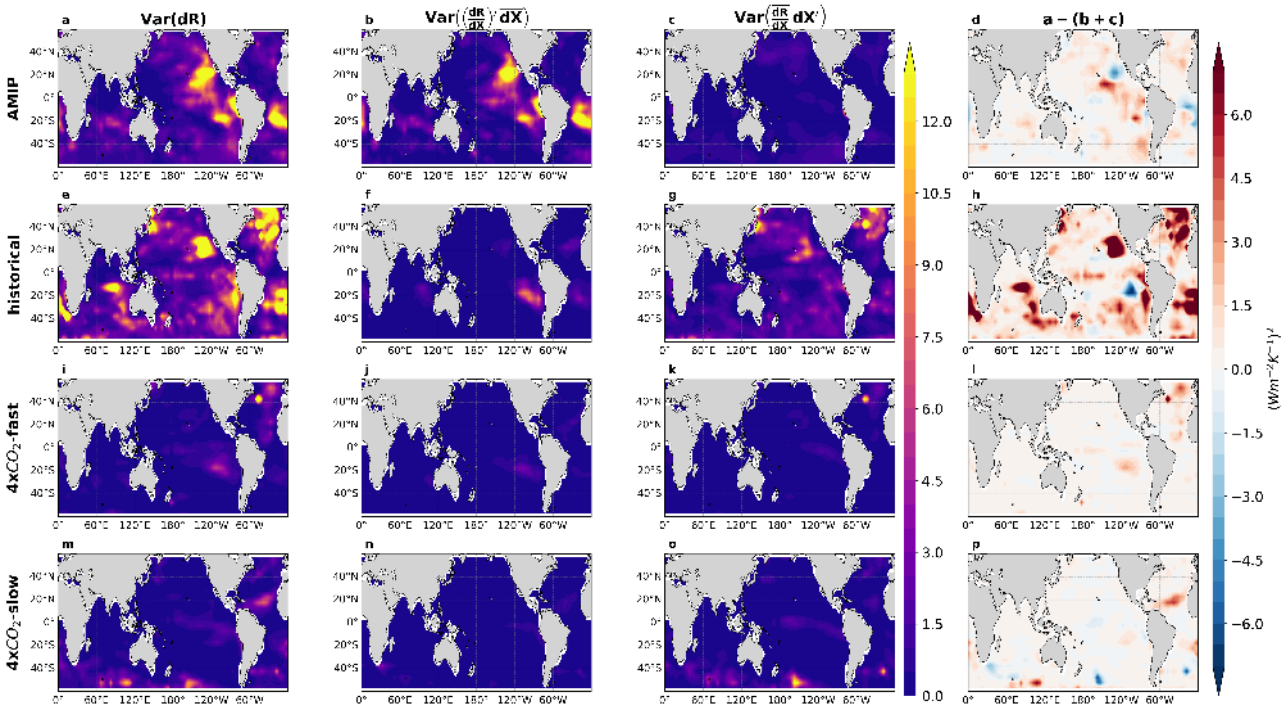

Figure D2. Same as Figure 4 on the spatial distribution of variance for each term in Equation 3 specific to EIS-induced feedback.

https://doi.org/10.5194/egusphere-2025-3177
Preprint. Discussion started: 11 July 2025

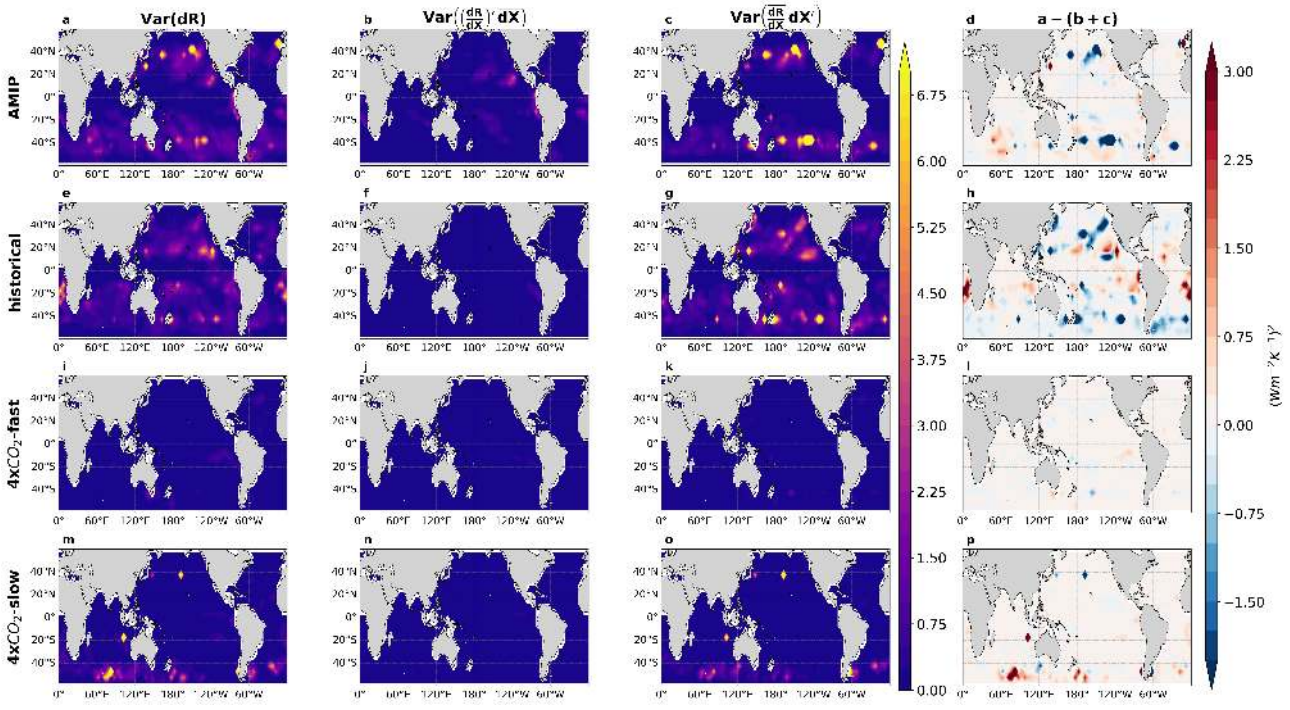

Figure D3. Same as Figure 4 on the spatial distribution of variance for each term in Equation 3 specific to T_{adv}-induced feedback.

https://doi.org/10.5194/egusphere-2025-3177
Preprint. Discussion started: 11 July 2025

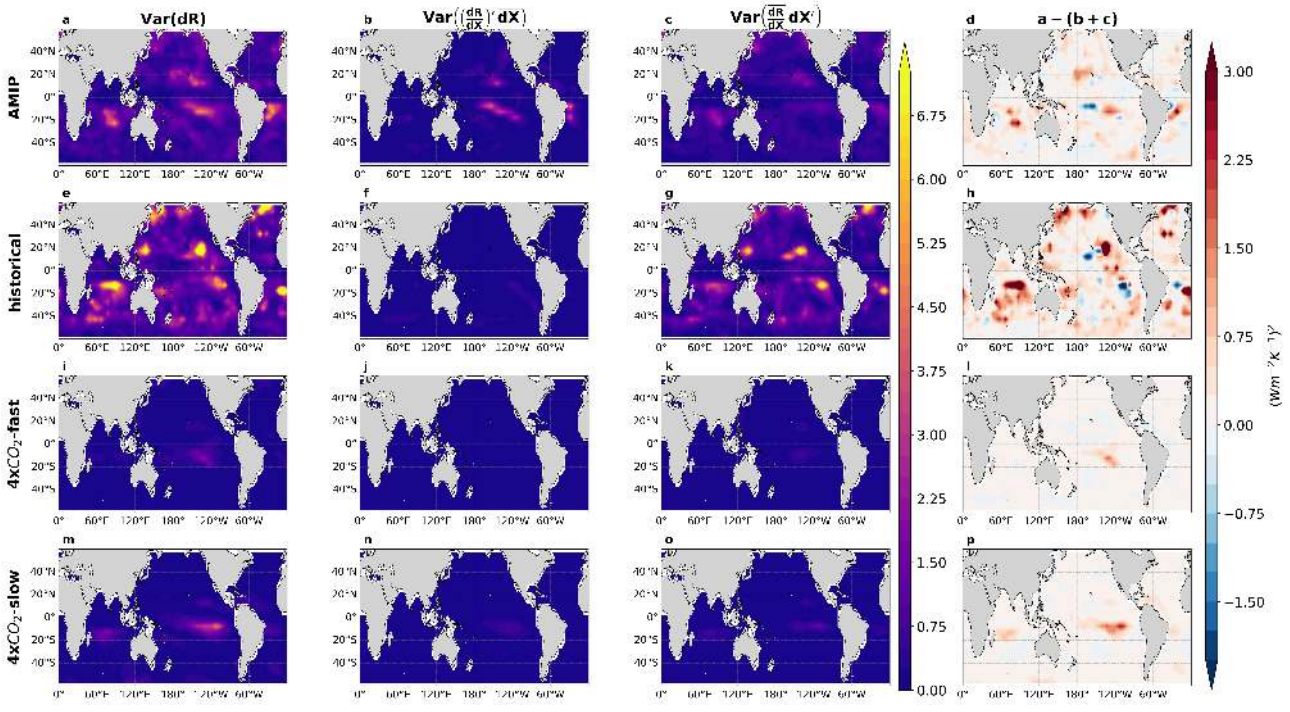

Figure D4. Same as Figure 4 on the spatial distribution of variance for each term in Equation 3 specific to RH-induced feedback.

https://doi.org/10.5194/egusphere-2025-3177
Preprint. Discussion started: 11 July 2025

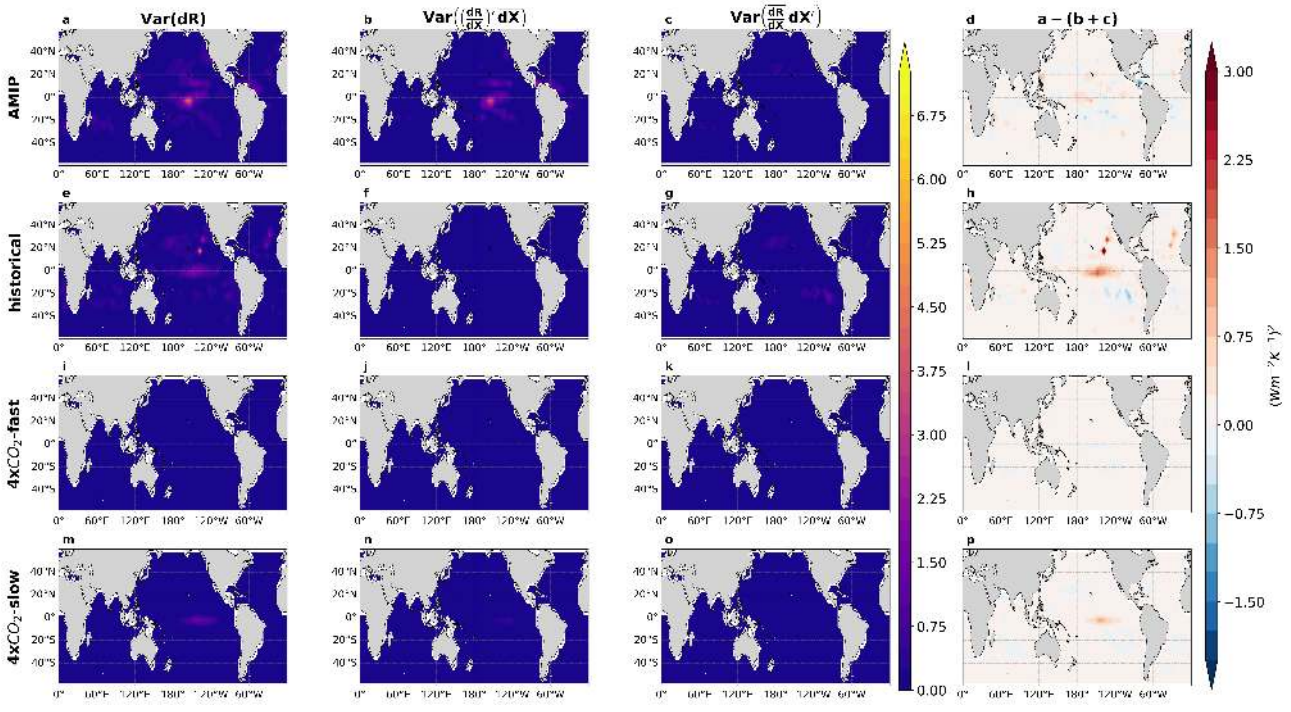

Figure D5. Same as Figure 4 on the spatial distribution of variance for each term in Equation 3 specific to ω-induced feedback.

https://doi.org/10.5194/egusphere-2025-3177
Preprint. Discussion started: 11 July 2025

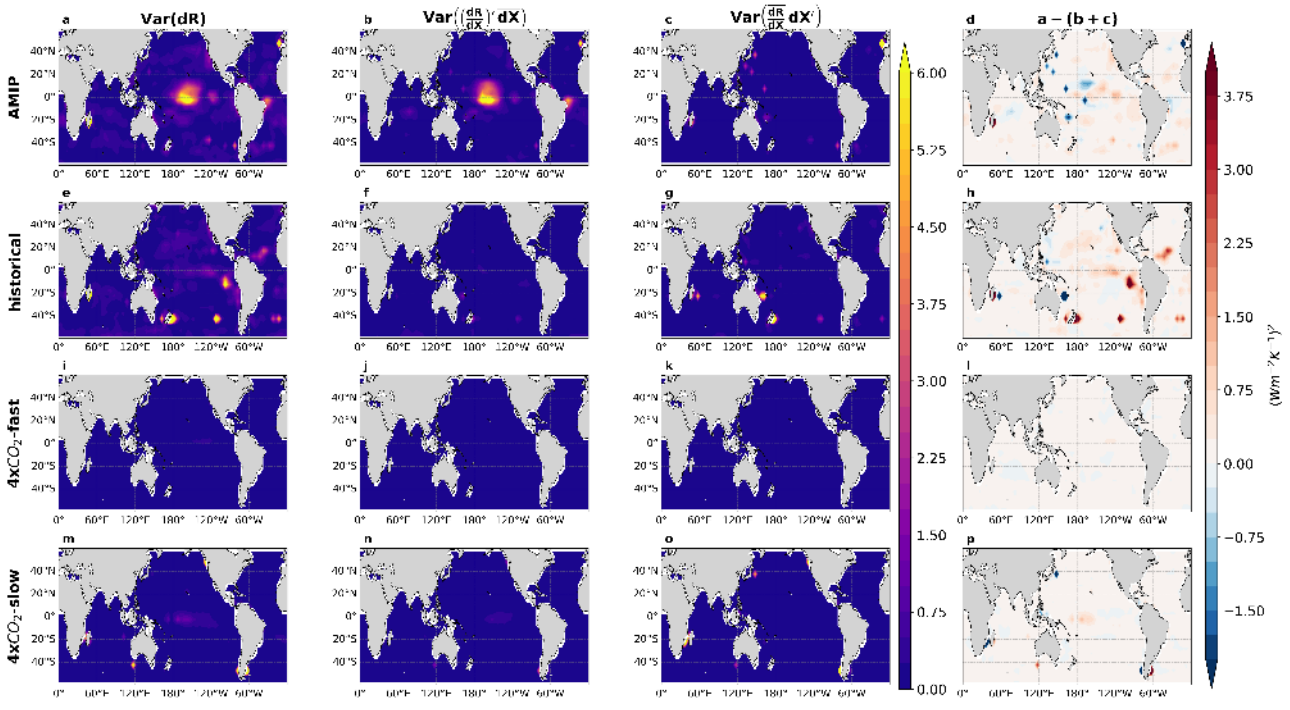

Figure D6. Same as Figure 4 on the spatial distribution of variance for each term in Equation 3 specific to WS-induced feedback.

https://doi.org/10.5194/egusphere-2025-3177
Preprint. Discussion started: 11 July 2025

Appendix E: CMIP Model Datasets Used

		AMIP (1982/01 - 2008/12)	Historical (1982/01 - 2008/12)	4xCO2 (Year 1 -150)
MIP Era	Model Name	References		
CMIP 6	CanESM5	Swart et al. (2019a)	Swart et al. (2019b)	Swart et al. (2019c)
	E3SM-1-0	Bader et al. (2019a)	Bader et al. (2019b)	Bader et al. (2019c)
	GFDL-CM4	Guo et al. (2018a)	Guo et al. (2018b)	Guo et al. (2018c)
	HadGEM3-GC31-LL	Ridley et al. (2019a)	Ridley et al. (2019b)	Ridley et al. (2019c)
	IPSL-CM6A-LR	Boucher et al. (2018a)	Boucher et al. (2018b)	Boucher et al. (2018c)
	MIROC-ES2L	Hajima et al. (2020)	Hajima et al. (2019a)	Hajima et al. (2019b)
	MIROC6	Tatebe and Watanabe (2018a)	Tatebe and Watanabe (2018b)	Tatebe and Watanabe (2018c)
	MRI-ESM2-0	Yukimoto et al. (2019a)	Yukimoto et al. (2019b)	Yukimoto et al. (2019c)
	UKESM1-0-LL	Tang et al. (2019a)	Tang et al. (2019b)	Tang et al. (2019c)
CMIP 5	CCSM4	Gent et al. (2011)		
	CanESM2 (CanAM4)	Von Salzen et al. (2013)		
	HadGEM2-ES	Bellouin N. et al, (2007), Collins W.J. et al, (2008), Martin et al. (2006), Johns et al. (2006), Ringer et al. (2006)		
	MIROC-ESM	Watanabe et al. (2011)		
	MIROC5	Watanabe et al. (2010)		
	MPI-ESM-LR	Raddatz et al. (2007)		
	MRI-CGCM3	Yukimoto et al. (2011)		

Table E1. References and the period used for each experiment from CMIP 5 and 6.

https://doi.org/10.5194/egusphere-2025-3177
Preprint. Discussion started: 11 July 2025

Appendix F: Summary of Near-global Total Low-cloud Feedback Estimates and their Sub-components

Feedback ($Wm^{-2}K^{-1}$)	AMIP		Hist		Fast		Slow	
Kernel*dCCF	Mean	SD	Mean	SD	Mean	SD	Mean	SD
Mod*Mod	-0.37	0.39	-0.04	0.44	0.13	0.36	0.29	0.34
CERES*Mod	-0.60	0.08	-0.07	0.28	0.13	0.10	0.38	0.10
MODIS*Mod	-0.95	0.13	-0.27	0.42	0.02	0.15	0.35	0.13
ISCCP*Mod	-0.61	0.13	-0.01	0.30	0.19	0.13	0.44	0.13
PATMOS*Mod	-0.23	0.12	0.23	0.26	0.33	0.12	0.58	0.18
Mod*MMM	-0.34	0.42	-0.01	0.46	0.13	0.38	0.28	0.36
MMM*Mod	-0.35	0.08	0.01	0.21	0.13	0.09	0.29	0.09
Obs-Mean	-0.60	0.25	-0.03	0.18	0.17	0.11	0.44	0.09
Mean	-0.51	0.24	-0.02	0.14	0.15	0.09	0.39	0.10

Table F1. Values for the ensemble mean (red diamonds in Figure 1 of near-global total low-cloud feedback estimates and their 1σ standard deviation (SD) per experiment calculated with various calculation combinations of radiative flux sensitivities to meteorology ($\partial R/\partial CCF$) and meteorological changes under warming ($dCCF/dT_g$). Each row represents a combination, where *Mod* stands for model-specific and *MMM* stands for ensemble mean. For example, *Mod*Mod* represents the product of model-specific kernels and model-specific meteorology, *MMM*Mod* stands for ensemble mean kernels and model-specific CCFs. In the last two rows, the **Mean** column of *Obs-Mean* average results across feedback estimates derived from observational kernels (CERES, MODIS, ISCCP and PATMOS-X), while *Mean* is the average feedback across all 7 estimates. **SD** column of those two rows is the 1σ standard deviation of across the 4/7 feedback estimates.

https://doi.org/10.5194/egusphere-2025-3177
Preprint. Discussion started: 11 July 2025

Author contributions. RYST designed and performed the analysis and wrote the manuscript. CP co-designed the analysis and edited the manuscript. All authors edited the manuscript.

Competing interests. The authors declare no competing interests.

Acknowledgements. RYST, YJL, KM, and CP were supported by Department of Energy (DOE) Award DE-SC0022110 through the Regional and Global Model Analysis (RGMA) program. MDZ's work was performed under the auspices of the United States Department of Energy (DOE) by Lawrence Livermore National Laboratory under contract no. DE-AC52-07NA27344 and was supported by the Regional and Global Model Analysis Program of the Office of Science at the DOE.

https://doi.org/10.5194/egusphere-2025-3177
Preprint. Discussion started: 11 July 2025

References

Andrews, T. and Ringer, M. A.: Cloud Feedbacks, Rapid Adjustments, and the Forcing–Response Relationship in a Transient CO2 Reversibility Scenario, Journal of Climate, 27, 1799–1818, https://doi.org/10.1175/JCLI-D-13-00421.1, 2014.

Andrews, T., Gregory, J. M., Webb, M. J., and Taylor, K. E.: Forcing, feedbacks and climate sensitivity in CMIP5 coupled atmosphere-ocean climate models: CLIMATE SENSITIVITY IN CMIP5 MODELS, Geophysical Research Letters, 39, n/a–n/a, https://doi.org/10.1029/2012GL051607, 2012.

Andrews, T., Gregory, J. M., and Webb, M. J.: The Dependence of Radiative Forcing and Feedback on Evolving Patterns of Surface Temperature Change in Climate Models, Journal of Climate, 28, 1630–1648, https://doi.org/10.1175/JCLI-D-14-00545.1, 2015.

Andrews, T., Gregory, J. M., Paynter, D., Silvers, L. G., Zhou, C., Mauritsen, T., Webb, M. J., Armour, K. C., Forster, P. M., and Titchner, H.: Accounting for Changing Temperature Patterns Increases Historical Estimates of Climate Sensitivity, Geophysical Research Letters, 45, 8490–8499, https://doi.org/10.1029/2018GL078887, 2018.

Andrews, T., BodasSalcedo, A., Gregory, J. M., Dong, Y., Armour, K. C., Paynter, D., Lin, P., Modak, A., Mauritsen, T., Cole, J. N. S., Medeiros, B., Benedict, J. J., Douville, H. e., Roehrig, R., Koshiro, T., Kawai, H., Ogura, T., Dufresne, J., Allan, R. P., and Liu, C.: On the Effect of Historical SST Patterns on Radiative Feedback, Journal of Geophysical Research: Atmospheres, 127, https://doi.org/10.1029/2022JD036675, 2022.

Armour, K. C.: Energy budget constraints on climate sensitivity in light of inconstant climate feedbacks, Nature Climate Change, 7, 331–335, https://doi.org/10.1038/nclimate3278, 2017.

Armour, K. C., Bitz, C. M., and Roe, G. H.: Time-Varying Climate Sensitivity from Regional Feedbacks, Journal of Climate, 26, 4518–4534, https://doi.org/10.1175/JCLI-D-12-00544.1, 2013.

Armour, K. C., Proistosescu, C., Dong, Y., Hahn, L. C., Blanchard-Wrigglesworth, E., Pauling, A. G., Jnglin Wills, R. C., Andrews, T., Stuecker, M. F., Po-Chedley, S., Mitevski, I., Forster, P. M., and Gregory, J. M.: Sea-surface temperature pattern effects have slowed global warming and biased warming-based constraints on climate sensitivity, Proceedings of the National Academy of Sciences, 121, e2312093 121, https://doi.org/10.1073/pnas.2312093121, 2024.

Bader, D. C., Leung, R., Taylor, M., and McCoy, R. B.: E3SM-Project E3SM1.0 model output prepared for CMIP6 CMIP amip, https://doi.org/10.22033/ESGF/CMIP6.4492, 2019a.

Bader, D. C., Leung, R., Taylor, M., and McCoy, R. B.: E3SM-Project E3SM1.0 model output prepared for CMIP6 CMIP historical, https://doi.org/10.22033/ESGF/CMIP6.4497, 2019b.

Bader, D. C., Leung, R., Taylor, M., and McCoy, R. B.: E3SM-Project E3SM1.0 model output prepared for CMIP6 CMIP abrupt-4xCO2, https://doi.org/10.22033/ESGF/CMIP6.4491, 2019c.

Bodas-Salcedo, A., Webb, M. J., Bony, S., Chepfer, H., Dufresne, J.-L., Klein, S. A., Zhang, Y., Marchand, R., Haynes, J. M., Pincus, R., and John, V. O.: COSP: Satellite simulation software for model assessment, Bulletin of the American Meteorological Society, 92, 1023–1043, https://doi.org/10.1175/2011BAMS2856.1, 2011.

Bony, S. and Dufresne, J.-L.: Marine boundary layer clouds at the heart of tropical cloud feedback uncertainties in climate models, Geophysical Research Letters, 32, L20 806, https://doi.org/10.1029/2005GL023851, 2005.

Boucher, O., Denvil, S., Levavasseur, G., Cozic, A., Caubel, A., Foujols, M.-A., Meurdesoif, Y., Cadule, P., Devilliers, M., Ghattas, J., Lebas, N., Lurton, T., Mellul, L., Musat, I., Mignot, J., Cheruy, F., Boucher, O., Denvil, S., Levavasseur, G., Cozic, A., Caubel, A., Foujols,

https://doi.org/10.5194/egusphere-2025-3177
Preprint. Discussion started: 11 July 2025

M.-A., Meurdesoif, Y., Cadule, P., Devilliers, M., Ghattas, J., Lebas, N., Lurton, T., Mellul, L., Musat, I., Mignot, J., and Cheruy, F.: IPSL IPSL-CM6A-LR model output prepared for CMIP6 CMIP amip, https://doi.org/10.22033/ESGF/CMIP6.5113, 2018a.

Boucher, O., Denvil, S., Levavasseur, G., Cozic, A., Caubel, A., Foujols, M.-A., Meurdesoif, Y., Cadule, P., Devilliers, M., Ghattas, J., Lebas, N., Lurton, T., Mellul, L., Musat, I., Mignot, J., Cheruy, F., Boucher, O., Denvil, S., Levavasseur, G., Cozic, A., Caubel, A., Foujols, M.-A., Meurdesoif, Y., Cadule, P., Devilliers, M., Ghattas, J., Lebas, N., Lurton, T., Mellul, L., Musat, I., Mignot, J., and Cheruy, F.: IPSL IPSL-CM6A-LR model output prepared for CMIP6 CMIP historical, https://doi.org/10.22033/ESGF/CMIP6.5195, 2018b.

Boucher, O., Denvil, S., Levavasseur, G., Cozic, A., Caubel, A., Foujols, M.-A., Meurdesoif, Y., Cadule, P., Devilliers, M., Ghattas, J., Lebas, N., Lurton, T., Mellul, L., Musat, I., Mignot, J., Cheruy, F., Boucher, O., Denvil, S., Levavasseur, G., Cozic, A., Caubel, A., Foujols, M.-A., Meurdesoif, Y., Cadule, P., Devilliers, M., Ghattas, J., Lebas, N., Lurton, T., Mellul, L., Musat, I., Mignot, J., and Cheruy, F.: IPSL IPSL-CM6A-LR model output prepared for CMIP6 CMIP abrupt-4xCO2, https://doi.org/10.22033/ESGF/CMIP6.5109, 2018c.

Bretherton, C. S.: Insights into low-latitude cloud feedbacks from high-resolution models, Philosophical Transactions of the Royal Society A: Mathematical, Physical and Engineering Sciences, 373, 20140 415, https://doi.org/10.1098/rsta.2014.0415, 2015.

Cesana, G. V. and Del Genio, A. D.: Observational constraint on cloud feedbacks suggests moderate climate sensitivity, Nature Climate Change, 11, 213–218, https://doi.org/10.1038/s41558-020-00970-y, 2021.

Copernicus Climate Change Service: ERA5 monthly averaged data on single levels from 1940 to present, https://doi.org/10.24381/CDS.F17050D7, 2019a.

Copernicus Climate Change Service: ERA5 monthly averaged data on pressure levels from 1940 to present, https://doi.org/10.24381/CDS.6860A573, 2019b.

Doelling, D.: CERES Monthly Daytime Mean Regionally Averaged Terra and Aqua TOA Fluxes and Associated Cloud Properties Stratified by Optical Depth and Effective Pressure Edition4A, https://doi.org/10.5067/TERRA-AQUA/CERES/FLUXBYCLDTYP-MONTH_L3.004A, 2020.

Dong, Y., Proistosescu, C., Armour, K. C., and Battisti, D. S.: Attributing Historical and Future Evolution of Radiative Feedbacks to Regional Warming Patterns using a Green's Function Approach: The Preeminence of the Western Pacific, Journal of Climate, 32, 5471–5491, https://doi.org/10.1175/JCLI-D-18-0843.1, 2019.

Dong, Y., Armour, K. C., Zelinka, M. D., Proistosescu, C., Battisti, D. S., Zhou, C., and Andrews, T.: Intermodel Spread in the Pattern Effect and Its Contribution to Climate Sensitivity in CMIP5 and CMIP6 Models, Journal of Climate, 33, 7755–7775, https://doi.org/10.1175/JCLI-D-19-1011.1, 2020.

Dong, Y., Armour, K. C., Proistosescu, C., Andrews, T., Battisti, D. S., Forster, P. M., Paynter, D., Smith, C. J., and Shiogama, H.: Biased Estimates of Equilibrium Climate Sensitivity and Transient Climate Response Derived From Historical CMIP6 Simulations, Geophysical Research Letters, 48, https://doi.org/10.1029/2021GL095778, 2021.

Eyring, V., Bony, S., Meehl, G. A., Senior, C. A., Stevens, B., Stouffer, R. J., and Taylor, K. E.: Overview of the Coupled Model Intercomparison Project Phase 6 (CMIP6) experimental design and organization, Geoscientific Model Development, 9, 1937–1958, https://doi.org/10.5194/gmd-9-1937-2016, 2016.

Gent, P. R., Danabasoglu, G., Donner, L. J., Holland, M. M., Hunke, E. C., Jayne, S. R., Lawrence, D. M., Neale, R. B., Rasch, P. J., Vertenstein, M., Worley, P. H., Yang, Z.-L., and Zhang, M.: The Community Climate System Model Version 4, Journal of Climate, 24, 4973–4991, https://doi.org/10.1175/2011JCLI4083.1, 2011.

Guo, H., John, J. G., Blanton, C., McHugh, C., Nikonov, S., Radhakrishnan, A., Rand, K., Zadeh, N. T., Balaji, V., Durachta, J., Dupuis, C., Menzel, R., Robinson, T., Underwood, S., Vahlenkamp, H., Bushuk, M., Dunne, K. A., Dussin, R., Gauthier, P. P., Ginoux, P., Griffies,

https://doi.org/10.5194/egusphere-2025-3177
Preprint. Discussion started: 11 July 2025

S. M., Hallberg, R., Harrison, M., Hurlin, W., Lin, P., Malyshev, S., Naik, V., Paulot, F., Paynter, D. J., Ploshay, J., Reichl, B. G., Schwarzkopf, D. M., Seman, C. J., Shao, A., Silvers, L., Wyman, B., Yan, X., Zeng, Y., Adcroft, A., Dunne, J. P., Held, I. M., Krasting, J. P., Horowitz, L. W., Milly, P., Shevliakova, E., Winton, M., Zhao, M., and Zhang, R.: NOAA-GFDL GFDL-CM4 model output amip, https://doi.org/10.22033/ESGF/CMIP6.8494, 2018a.

Guo, H., John, J. G., Blanton, C., McHugh, C., Nikonov, S., Radhakrishnan, A., Rand, K., Zadeh, N. T., Balaji, V., Durachta, J., Dupuis, C., Menzel, R., Robinson, T., Underwood, S., Vahlenkamp, H., Bushuk, M., Dunne, K. A., Dussin, R., Gauthier, P. P., Ginoux, P., Griffies, S. M., Hallberg, R., Harrison, M., Hurlin, W., Lin, P., Malyshev, S., Naik, V., Paulot, F., Paynter, D. J., Ploshay, J., Reichl, B. G., Schwarzkopf, D. M., Seman, C. J., Shao, A., Silvers, L., Wyman, B., Yan, X., Zeng, Y., Adcroft, A., Dunne, J. P., Held, I. M., Krasting, J. P., Horowitz, L. W., Milly, P., Shevliakova, E., Winton, M., Zhao, M., and Zhang, R.: NOAA-GFDL GFDL-CM4 model output historical, https://doi.org/10.22033/ESGF/CMIP6.8594, 2018b.

Guo, H., John, J. G., Blanton, C., McHugh, C., Nikonov, S., Radhakrishnan, A., Rand, K., Zadeh, N. T., Balaji, V., Durachta, J., Dupuis, C., Menzel, R., Robinson, T., Underwood, S., Vahlenkamp, H., Bushuk, M., Dunne, K. A., Dussin, R., Gauthier, P. P., Ginoux, P., Griffies, S. M., Hallberg, R., Harrison, M., Hurlin, W., Lin, P., Malyshev, S., Naik, V., Paulot, F., Paynter, D. J., Ploshay, J., Reichl, B. G., Schwarzkopf, D. M., Seman, C. J., Shao, A., Silvers, L., Wyman, B., Yan, X., Zeng, Y., Adcroft, A., Dunne, J. P., Held, I. M., Krasting, J. P., Horowitz, L. W., Milly, P., Shevliakova, E., Winton, M., Zhao, M., and Zhang, R.: NOAA-GFDL GFDL-CM4 model output abrupt-4xCO2, https://doi.org/10.22033/ESGF/CMIP6.8486, 2018c.

Hajima, T., Abe, M., Arakawa, O., Suzuki, T., Komuro, Y., Ogura, T., Ogochi, K., Watanabe, M., Yamamoto, A., Tatebe, H., Noguchi, M. A., Ohgaito, R., Ito, A., Yamazaki, D., Ito, A., Takata, K., Watanabe, S., Kawamiya, M., and Tachiiri, K.: MIROC MIROC-ES2L model output prepared for CMIP6 CMIP historical, https://doi.org/10.22033/ESGF/CMIP6.5602, 2019a.

Hajima, T., Abe, M., Arakawa, O., Suzuki, T., Komuro, Y., Ogura, T., Ogochi, K., Watanabe, M., Yamamoto, A., Tatebe, H., Noguchi, M. A., Ohgaito, R., Ito, A., Yamazaki, D., Ito, A., Takata, K., Watanabe, S., Kawamiya, M., and Tachiiri, K.: MIROC MIROC-ES2L model output prepared for CMIP6 CMIP abrupt-4xCO2, https://doi.org/10.22033/ESGF/CMIP6.5410, 2019b.

Hajima, T., Abe, M., Arakawa, O., Suzuki, T., Komuro, Y., Ogura, T., Ogochi, K., Watanabe, M., Yamamoto, A., Tatebe, H., Noguchi, M. A., Ohgaito, R., Ito, A., Yamazaki, D., Ito, A., Takata, K., Watanabe, S., Kawamiya, M., and Tachiiri, K.: MIROC MIROC-ES2L model output prepared for CMIP6 CMIP amip, https://doi.org/10.22033/ESGF/CMIP6.5421, 2020.

Heidinger, A. K., Foster, M. J., Walther, A., and Zhao, X. T.: The Pathfinder Atmospheres–Extended AVHRR Climate Dataset, Bulletin of the American Meteorological Society, 95, 909–922, https://doi.org/10.1175/BAMS-D-12-00246.1, 2014.

Held, I. M., Winton, M., Takahashi, K., Delworth, T., Zeng, F., and Vallis, G. K.: Probing the Fast and Slow Components of Global Warming by Returning Abruptly to Preindustrial Forcing, Journal of Climate, 23, 2418–2427, https://doi.org/10.1175/2009JCLI3466.1, 2010.

Huang, B., Liu, C., Banzon, V., Freeman, E., Graham, G., Hankins, B., Smith, T., and Zhang, H.-M.: Improvements of the Daily Optimum Interpolation Sea Surface Temperature (DOISST) Version 2.1, Journal of Climate, 34, 2923–2939, https://doi.org/10.1175/JCLI-D-20-0166.1, 2021.

Johns, T. C., Durman, C. F., Banks, H. T., Roberts, M. J., McLaren, A. J., Ridley, J. K., Senior, C. A., Williams, K. D., Jones, A., Rickard, G. J., Cusack, S., Ingram, W. J., Crucifix, M., Sexton, D. M. H., Joshi, M. M., Dong, B.-W., Spencer, H., Hill, R. S. R., Gregory, J. M., Keen, A. B., Pardaens, A. K., Lowe, J. A., Bodas-Salcedo, A., Stark, S., and Searl, Y.: The New Hadley Centre Climate Model (HadGEM1): Evaluation of Coupled Simulations, Journal of Climate, 19, 1327–1353, https://doi.org/10.1175/JCLI3712.1, 2006.

Klein, S. A., Hall, A., Norris, J. R., and Pincus, R.: Low-Cloud Feedbacks from Cloud-Controlling Factors: A Review, Surveys in Geophysics, 38, 1307–1329, https://doi.org/10.1007/s10712-017-9433-3, 2017.

https://doi.org/10.5194/egusphere-2025-3177
Preprint. Discussion started: 11 July 2025

Lewis, H., Bellon, G., and Dinh, T.: Upstream Large-Scale Control of Subtropical Low-Cloud Climatology, Journal of Climate, 36, 3289–3303, https://doi.org/10.1175/JCLI-D-22-0676.1, 2023.

Lilly, D. K.: Models of cloud-topped mixed layers under a strong inversion, Quarterly Journal of the Royal Meteorological Society, 94, 292–309, https://doi.org/10.1002/qj.49709440106, 1968.

Lin, Y.-J., Cesana, G. V., Proistosescu, C., Zelinka, M. D., and Armour, K. C.: The Relative Importance of Forced and Unforced Temperature Patterns in Driving the Time Variation of Low-Cloud Feedback, Journal of Climate, 38, 513–529, https://doi.org/10.1175/JCLI-D-24-0014.1, 2025.

Martin, G. M., Ringer, M. A., Pope, V. D., Jones, A., Dearden, C., and Hinton, T. J.: The Physical Properties of the Atmosphere in the New Hadley Centre Global Environmental Model (HadGEM1). Part I: Model Description and Global Climatology, Journal of Climate, 19, 1274–1301, https://doi.org/10.1175/JCLI3636.1, 2006.

Mauger, G. S. and Norris, J. R.: Assessing the Impact of Meteorological History on Subtropical Cloud Fraction, Journal of Climate, 23, 2926–2940, https://doi.org/10.1175/2010JCLI3272.1, 2010.

Myers, T. A. and Norris, J. R.: On the Relationships between Subtropical Clouds and Meteorology in Observations and CMIP3 and CMIP5 Models, Journal of Climate, 28, 2945–2967, https://doi.org/10.1175/JCLI-D-14-00475.1, 2015.

Myers, T. A., Scott, R. C., Zelinka, M. D., Klein, S. A., Norris, J. R., and Caldwell, P. M.: Observational constraints on low cloud feedback reduce uncertainty of climate sensitivity, Nature Climate Change, 11, 501–507, https://doi.org/10.1038/s41558-021-01039-0, 2021.

Myers, T. A., Zelinka, M. D., and Klein, S. A.: Observational Constraints on the Cloud Feedback Pattern Effect, Journal of Climate, pp. 1–31, https://doi.org/10.1175/JCLI-D-22-0862.1, 2023.

Pincus, R., Baker, M. B., and Bretherton, C. S.: What Controls Stratocumulus Radiative Properties? Lagrangian Observations of Cloud Evolution, Journal of the Atmospheric Sciences, 54, 2215–2236, https://doi.org/10.1175/1520-0469(1997)054<2215:WCSRPL>2.0.CO;2, 1997.

Platnick, S., S. A. A. M. D. K. K. M. W. P. M. R. E. H. B. A. B. and Yang, P.: MODIS atmosphere L2 cloud product (06 L2), NASA MODIS Adaptive Processing System, Goddard Space Flight Center, https://doi.org/10.5067/MODIS/MOD06_L2.006, 2015.

Proistosescu, C. and Huybers, P. J.: Slow climate mode reconciles historical and model-based estimates of climate sensitivity, Science Advances, 3, e1602 821, https://doi.org/10.1126/sciadv.1602821, 2017.

Proistosescu, C., Donohoe, A., Armour, K. C., Roe, G. H., Stuecker, M. F., and Bitz, C. M.: Radiative feedbacks from stochastic variability in surface temperature and radiative imbalance, Geophysical Research Letters, 45, 5082–5094, 2018.

Raddatz, T. J., Reick, C. H., Knorr, W., Kattge, J., Roeckner, E., Schnur, R., Schnitzler, K.-G., Wetzel, P., and Jungclaus, J.: Will the tropical land biosphere dominate the climate–carbon cycle feedback during the twenty-first century?, Climate Dynamics, 29, 565–574, https://doi.org/10.1007/s00382-007-0247-8, 2007.

Ridley, J., Menary, M., Kuhlbrodt, T., Andrews, M., and Andrews, T.: MOHC HadGEM3-GC31-LL model output prepared for CMIP6 CMIP amip, https://doi.org/10.22033/ESGF/CMIP6.5853, 2019a.

Ridley, J., Menary, M., Kuhlbrodt, T., Andrews, M., and Andrews, T.: MOHC HadGEM3-GC31-LL model output prepared for CMIP6 CMIP historical, https://doi.org/10.22033/ESGF/CMIP6.6109, 2019b.

Ridley, J., Menary, M., Kuhlbrodt, T., Andrews, M., and Andrews, T.: MOHC HadGEM3-GC31-LL model output prepared for CMIP6 CMIP abrupt-4xCO2, https://doi.org/10.22033/ESGF/CMIP6.5839, 2019c.

https://doi.org/10.5194/egusphere-2025-3177
Preprint. Discussion started: 11 July 2025

Ringer, M. A., Martin, G. M., Greeves, C. Z., Hinton, T. J., James, P. M., Pope, V. D., Scaife, A. A., Stratton, R. A., Inness, P. M., Slingo, J. M., and Yang, G.-Y.: The Physical Properties of the Atmosphere in the New Hadley Centre Global Environmental Model (HadGEM1). Part II: Aspects of Variability and Regional Climate, Journal of Climate, 19, 1302–1326, https://doi.org/10.1175/JCLI3713.1, 2006.

Rossow, W., Golea, V., Walker, A., Knapp, K., Young, A., Hankins, B., and Inamdar, A.: International Satellite Cloud Climatology Project (ISCCP) Climate Data Record, H-Series, https://doi.org/10.7289/V5QZ281S, 2017.

Scott, R. C., Myers, T. A., Norris, J. R., Zelinka, M. D., Klein, S. A., Sun, M., and Doelling, D. R.: Observed Sensitivity of Low-Cloud Radiative Effects to Meteorological Perturbations over the Global Oceans, Journal of Climate, 33, 7717–7734, https://doi.org/10.1175/JCLI-D-19-1028.1, 2020.

Senior, C. A. and Mitchell, J. F. B.: The time-dependence of climate sensitivity, Geophysical Research Letters, 27, 2685–2688, https://doi.org/10.1029/2000GL011373, 2000.

Sherwood, S. C., Webb, M. J., Annan, J. D., Armour, K. C., Forster, P. M., Hargreaves, J. C., Hegerl, G., Klein, S. A., Marvel, K. D., Rohling, E. J., Watanabe, M., Andrews, T., Braconnot, P., Bretherton, C. S., Foster, G. L., Hausfather, Z., Heydt, A. S., Knutti, R., Mauritsen, T., Norris, J. R., Proistosescu, C., Rugenstein, M., Schmidt, G. A., Tokarska, K. B., and Zelinka, M. D.: An Assessment of Earth's Climate Sensitivity Using Multiple Lines of Evidence, Reviews of Geophysics, 58, https://doi.org/10.1029/2019RG000678, 2020.

Swart, N. C., Cole, J. N., Kharin, V. V., Lazare, M., Scinocca, J. F., Gillett, N. P., Anstey, J., Arora, V., Christian, J. R., Jiao, Y., Lee, W. G., Majaess, F., Saenko, O. A., Seiler, C., Seinen, C., Shao, A., Solheim, L., von Salzen, K., Yang, D., Winter, B., and Sigmond, M.: CCCma CanESM5 model output prepared for CMIP6 CMIP amip, https://doi.org/10.22033/ESGF/CMIP6.3535, 2019a.

Swart, N. C., Cole, J. N., Kharin, V. V., Lazare, M., Scinocca, J. F., Gillett, N. P., Anstey, J., Arora, V., Christian, J. R., Jiao, Y., Lee, W. G., Majaess, F., Saenko, O. A., Seiler, C., Seinen, C., Shao, A., Solheim, L., von Salzen, K., Yang, D., Winter, B., and Sigmond, M.: CCCma CanESM5 model output prepared for CMIP6 CMIP historical, https://doi.org/10.22033/ESGF/CMIP6.3610, 2019b.

Swart, N. C., Cole, J. N., Kharin, V. V., Lazare, M., Scinocca, J. F., Gillett, N. P., Anstey, J., Arora, V., Christian, J. R., Jiao, Y., Lee, W. G., Majaess, F., Saenko, O. A., Seiler, C., Seinen, C., Shao, A., Solheim, L., von Salzen, K., Yang, D., Winter, B., and Sigmond, M.: CCCma CanESM5 model output prepared for CMIP6 CMIP abrupt-4xCO2, https://doi.org/10.22033/ESGF/CMIP6.3532, 2019c.

Tang, Y., Rumbold, S., Ellis, R., Kelley, D., Mulcahy, J., Sellar, A., Walton, J., and Jones, C.: MOHC UKESM1.0-LL model output prepared for CMIP6 CMIP amip, https://doi.org/10.22033/ESGF/CMIP6.5857, 2019a.

Tang, Y., Rumbold, S., Ellis, R., Kelley, D., Mulcahy, J., Sellar, A., Walton, J., and Jones, C.: MOHC UKESM1.0-LL model output prepared for CMIP6 CMIP historical, https://doi.org/10.22033/ESGF/CMIP6.6113, 2019b.

Tang, Y., Rumbold, S., Ellis, R., Kelley, D., Mulcahy, J., Sellar, A., Walton, J., and Jones, C.: MOHC UKESM1.0-LL model output prepared for CMIP6 CMIP abrupt-4xCO2, https://doi.org/10.22033/ESGF/CMIP6.5843, 2019c.

Tatebe, H. and Watanabe, M.: MIROC MIROC6 model output prepared for CMIP6 CMIP amip, https://doi.org/10.22033/ESGF/CMIP6.5422, 2018a.

Tatebe, H. and Watanabe, M.: MIROC MIROC6 model output prepared for CMIP6 CMIP historical, https://doi.org/10.22033/ESGF/CMIP6.5603, 2018b.

Tatebe, H. and Watanabe, M.: MIROC MIROC6 model output prepared for CMIP6 CMIP abrupt-4xCO2, https://doi.org/10.22033/ESGF/CMIP6.5411, 2018c.

Taylor, K. E., Stouffer, R. J., and Meehl, G. A.: An Overview of CMIP5 and the Experiment Design, Bulletin of the American Meteorological Society, 93, 485–498, https://doi.org/10.1175/BAMS-D-11-00094.1, 2012.

https://doi.org/10.5194/egusphere-2025-3177
Preprint. Discussion started: 11 July 2025

Von Salzen, K., Scinocca, J. F., McFarlane, N. A., Li, J., Cole, J. N. S., Plummer, D., Verseghy, D., Reader, M. C., Ma, X., Lazare, M., and Solheim, L.: The Canadian Fourth Generation Atmospheric Global Climate Model (CanAM4). Part I: Representation of Physical Processes, Atmosphere-Ocean, 51, 104–125, https://doi.org/10.1080/07055900.2012.755610, 2013.

Watanabe, M., Suzuki, T., O'ishi, R., Komuro, Y., Watanabe, S., Emori, S., Takemura, T., Chikira, M., Ogura, T., Sekiguchi, M., Takata, K., Yamazaki, D., Yokohata, T., Nozawa, T., Hasumi, H., Tatebe, H., and Kimoto, M.: Improved Climate Simulation by MIROC5: Mean States, Variability, and Climate Sensitivity, Journal of Climate, 23, 6312–6335, https://doi.org/10.1175/2010JCLI3679.1, 2010.

Watanabe, S., Hajima, T., Sudo, K., Nagashima, T., Takemura, T., Okajima, H., Nozawa, T., Kawase, H., Abe, M., Yokohata, T., Ise, T., Sato, H., Kato, E., Takata, K., Emori, S., and Kawamiya, M.: MIROC-ESM: model description and basic results of CMIP5-20c3m experiments, https://doi.org/10.5194/gmdd-4-1063-2011, 2011.

Wills, R. C. J., Dong, Y., Proistosecu, C., Armour, K. C., and Battisti, D. S.: Systematic Climate Model Biases in the LargeScale Patterns of Recent SeaSurface Temperature and SeaLevel Pressure Change, Geophysical Research Letters, 49, https://doi.org/10.1029/2022GL100011, 2022.

Yukimoto, S., Yoshimura, H., Hosaka, M., Sakami, T., Tsujino, H., Hirabara, M., Tanaka, T. Y., Deushi, M., Obata, A., Nakano, H., Adachi, Y., Shindo, E., Yabu, S., Ose, T., and Kitoh, A.: Meteorological Research Institute-Earth System Model Version 1 (MRI-ESM1) -Model Description-, https://doi.org/10.11483/mritechrepo.64, 2011.

Yukimoto, S., Koshiro, T., Kawai, H., Oshima, N., Yoshida, K., Urakawa, S., Tsujino, H., Deushi, M., Tanaka, T., Hosaka, M., Yoshimura, H., Shindo, E., Mizuta, R., Ishii, M., Obata, A., and Adachi, Y.: MRI MRI-ESM2.0 model output prepared for CMIP6 CMIP amip, https://doi.org/10.22033/ESGF/CMIP6.6758, 2019a.

Yukimoto, S., Koshiro, T., Kawai, H., Oshima, N., Yoshida, K., Urakawa, S., Tsujino, H., Deushi, M., Tanaka, T., Hosaka, M., Yoshimura, H., Shindo, E., Mizuta, R., Ishii, M., Obata, A., and Adachi, Y.: MRI MRI-ESM2.0 model output prepared for CMIP6 CMIP historical, https://doi.org/10.22033/ESGF/CMIP6.6842, 2019b.

Yukimoto, S., Koshiro, T., Kawai, H., Oshima, N., Yoshida, K., Urakawa, S., Tsujino, H., Deushi, M., Tanaka, T., Hosaka, M., Yoshimura, H., Shindo, E., Mizuta, R., Ishii, M., Obata, A., and Adachi, Y.: MRI MRI-ESM2.0 model output prepared for CMIP6 CMIP abrupt-4xCO2, https://doi.org/10.22033/ESGF/CMIP6.6755, 2019c.

Zelinka, M. D., Klein, S. A., and Hartmann, D. L.: Computing and Partitioning Cloud Feedbacks Using Cloud Property Histograms. Part II: Attribution to Changes in Cloud Amount, Altitude, and Optical Depth, Journal of Climate, 25, 3736–3754, https://doi.org/10.1175/JCLI-D-11-00249.1, 2012.

Zelinka, M. D., Myers, T. A., McCoy, D. T., PoChedley, S., Caldwell, P. M., Ceppi, P., Klein, S. A., and Taylor, K. E.: Causes of Higher Climate Sensitivity in CMIP6 Models, Geophysical Research Letters, 47, https://doi.org/10.1029/2019GL085782, 2020.

Zhou, C., Zelinka, M. D., Dessler, A. E., and Yang, P.: An Analysis of the Short-Term Cloud Feedback Using MODIS Data, Journal of Climate, 26, 4803–4815, https://doi.org/10.1175/JCLI-D-12-00547.1, 2013.

Zhou, C., Zelinka, M. D., and Klein, S. A.: Impact of decadal cloud variations on the Earth's energy budget, Nature Geoscience, 9, 871–874, https://doi.org/10.1038/ngeo2828, 2016.

Zhou, C., Zelinka, M. D., and Klein, S. A.: Analyzing the dependence of global cloud feedback on the spatial pattern of sea surface temperature change with a G reen's function approach, Journal of Advances in Modeling Earth Systems, 9, 2174–2189, https://doi.org/10.1002/2017MS001096, 2017.